Self-consistent simulations and analysis of the coupled-bunch instability for arbitrary multibunch configurations

Gabriele Bassi,[*] Alexei Blednykh, and Victor Smaluk

Brookhaven National Laboratory, Upton, New York 11973-5000, USA
(Received 13 November 2015; published 24 February 2016)

A novel algorithm for self-consistent simulations of long-range wakefield effects has been developed and applied to the study of both longitudinal and transverse coupled-bunch instabilities at NSLS-II. The algorithm is implemented in the new parallel tracking code SPACE (self-consistent parallel algorithm for collective effects) discussed in the paper. The code is applicable for accurate beam dynamics simulations in cases where both bunch-to-bunch and intrabunch motions need to be taken into account, such as chromatic head-tail effects on the coupled-bunch instability of a beam with a nonuniform filling pattern, or multibunch and single-bunch effects of a passive higher-harmonic cavity. The numerical simulations have been compared with analytical studies. For a beam with an arbitrary filling pattern, intensity-dependent complex frequency shifts have been derived starting from a system of coupled Vlasov equations. The analytical formulas and numerical simulations confirm that the analysis is reduced to the formulation of an eigenvalue problem based on the known formulas of the complex frequency shifts for the uniform filling pattern case.

I. INTRODUCTION

Beam dynamics simulations of collective effects can be computationally very demanding, and often numeric codes require powerful computer clusters to alleviate the computational load. This is evident when the code has to model the self-consistent dynamics of a large number of bunches interacting simultaneously via short- and long-range wakefields. In particular, time domain calculations of arbitrary long-range wakefield effects can be, besides time consuming, very memory demanding, since the algorithm requires to store the "history" of the bunches for several revolutions in order to calculate the wake forces at the present time. In many applications, such as passive higher-harmonic cavity operations, one cannot rely on point bunch approximations and has to follow the dynamics of the internal structure of the bunches and take into account transient effects. Another important application that requires efficient computational algorithms is the study of the coupled-bunch instability induced by the long-range interaction of bunches in arbitrary filling patterns. The accurate and efficient modeling of the aforementioned effects has motivated the development of the parallel tracking code SPACE discussed in this paper, where a novel self-consistent algorithm for the simulation of long-range effects induced by arbitrary wakefields is described in detail, and applied to the study

of the coupled-bunch instability in the NSLS-II storage ring for nonuniform filling patterns.

Several codes are available to simulate self-consistently single-bunch collective effects, however the availability of codes that simulate accurately multibunch effects is scarce, due to the complexity of the algorithm required to model long-range effects, and to the heavy computational load and memory requirements involved. Single-bunch numeric codes can have computational issues as well, when applied, for example, to dedicated studies such as the longitudinal microwave instability, where a large number of simulation particles is needed to study the response of small-scale bunch structures to high frequency wakefield components; if not equipped with suitable algorithms (i.e., smoothing/filtering techniques if based on particle methods, fine grids, parallel algorithms, etc.), single-bunch numeric codes can fail to produce reliable results. Coupled-bunch algorithms to various degree of self-consistency are implemented in [1–8]. Here we would like to mention MBTRACK, the code developed by Nagaoka *et al.* [4,5]. The idea behind our coupled-bunch algorithm, first discussed in our seminal paper [9], has been implemented in MBTRACK to model passive higher-harmonic cavity effects [10]. For a detailed description of the most recent method implemented in MBTRACK see [5].

SPACE has already accomplished some of its goals, such as the capability to simulate transient beam loading, passive higher-harmonic cavity effects, and coupled-bunch instabilities in arbitrary filling patterns, with the implementation of algorithms to model ion effects, low level rf and transverse feedback systems in progress. The first part of this paper is devoted to a detailed description of the

---

[*]gbassi@bnl.gov

algorithms implemented in SPACE. A short outline of the algorithm for the calculation of long-range wakefield effects has been given first in [9], followed by a more detailed description presented in [11,12]. Numerical simulations with SPACE have been performed for the NSLS-II storage ring in the study of the longitudinal microwave instability [14], in the study of passive higher-harmonic cavity effects [9,15], and in the analysis of coupled bunch instabilities driven by the higher order modes (HOMs) of a seven-cell PETRA-III rf cavity structure [11,16]. The analysis, based on self-consistent simulations of the slow head-tail damping to cure the coupled-bunch instability, has helped the transition to the next commissioning phase of the NSLS-II storage ring [11]. The coupled bunch instabilities, observed during commissioning with a gap in the filling patterns, have been analyzed theoretically and numerically assuming a uniform filling pattern. To investigate the validity of this assumption, we present an analytical treatment of the coupled-bunch instability for arbitrary filling patterns. The treatment is based on the formulation of an eigenvalue problem defined by the complex frequency shifts of the uniform filling pattern case. The numerical solution of the eigenvalue problem allows the study of instability thresholds via the determination of the eigenvalue with the largest imaginary part. As an application of the eigenvalue formulation, we foresee very fast schemes for the analysis of stable multibunch configurations, however, we believe that self-consistent numerical simulations add further robustness to the analysis, particularly if there is interest in the study of regimes far away from stability.

The paper is organized as follows. In Sec. II we describe the model used by SPACE for single and coupled-bunch instability simulations, and its method of solution, with particular emphasis on the novel algorithm for the calculation of the long-range wakefield interaction. In Sec. III we discuss the analytical treatment of the coupled-bunch instability that leads to the formulation of the eigenvalue problem for arbitrary filling patterns, and in Sec. IV we benchmark the analytical results against SPACE simulations, with application to the coupled-bunch instability in the NSLS-II storage ring. As a complementary tool to the computation of the eigenvalue spectrum, we discuss and apply the Gerschgorin circle theorem, useful for a rapid localization of the eigenvalues in the complex plane, and very effective for perturbative studies of uniform filling patterns.

II. SPACE CODE

SPACE is a parallel code for beam dynamics simulations of collective effects driven by short- and long-range wakefields. It is a Vlasov-Fokker-Planck solver based on a particle method, where M bunches, each with N_p simulation particles, to be distinguished from the actual number of particles in the bunch N_m ($m = 0, ..., M - 1$) [17], are

tracked according to a system of M-coupled Vlasov-Fokker-Planck equations. The terminology simulation particles is used, instead of macroparticles, since SPACE is based on a mean-field theory or Vlasov approach. Two distinct methods of solution of the Vlasov-Fokker-Planck equation are the particle method, implemented in SPACE, and the method based on the direct evolution of the phase space density, often called direct Vlasov solver [18,19]. For a discussion in the context of a two-dimensional Vlasov-Maxwell system see [20,21]. In a particle method, a condition for the numerical convergence to the solution of the Vlasov-Fokker-Planck system is achieved in the limit $N_p \rightarrow \infty$. For the determination of the wake forces, our particle method requires the estimation of one-dimensional (longitudinal) distribution densities, obtained via projection from the scattered phase space coordinates of the simulation particles. We therefore achieve numerical convergence by adding the limit $\Delta \rightarrow 0$, where Δ is the step size of the longitudinal grid used to construct the wake forces. We call it "weak" numerical convergence. A "strong" numerical convergence is achieved when the numerical accuracy is demanded on the phase-space densities Ψ_m, solution of the Vlasov-Fokker-Planck system of equations, a feature required by direct Vlasov solvers. Of course, particle methods can as well achieve a strong numerical convergence at the cost of suitably increasing the number of simulation particles N_p. To this end, powerful density estimation techniques should be employed [21].

SPACE has the capability to solve the single particle equations of motion via uploading a general 6×6 transfer map or by the use of a symplectic integrator. For dedicated studies such as the influence of the slow head-tail damping on the decoherence with amplitude process [22], the single particle dynamics is modeled with the addition of tune shift with amplitude coefficients. Wakefields can be modeled analytically or uploaded as input files if calculated numerically.

In many applications of interest, such as the study of the slow head-tail damping to cure coupled-bunch instabilities [11], it is a good approximation to model the single particle dynamics with a linear one-turn map defined by the knowledge on the betatron tunes and linear chromaticity, and to model collective effects via perturbing the particle momentum at each turn with kicks proportional to the local beta function for localized wakefields or impedances, and proportional to a constant beta function defined by the betatron tune for a global impedance distributed along the ring. We will discuss this case as an example of the model implemented in SPACE to study short- and long-range wakefield effects.

A. Vlasov-Fokker-Planck system

We consider M equidistant bunches with N_m particles ($m = 0, ..., M - 1$), circulating in the storage ring and satisfying the condition $M \leq h$, where h is the number

of rf buckets, with the reference particles of the bunches separated by the distance $d = C/M$, where C is the ring circumference. We assume the longitudinal motion of the bunches bounded around their reference particle position over a distance much shorter than d. For the evolution of the phase space density Ψ_m associated to the mth bunch, we consider the following system of M-coupled Vlasov-Fokker-Planck equations,

$$\frac{\partial \Psi_m}{\partial t} + (L_H + L_{FP} + L_C)\Psi_m = 0,$$
$$m = 0, \ldots, M - 1, \tag{1}$$

where

$$L_H = -\eta\delta\frac{\partial}{\partial\tau} + \frac{eV_{rf}}{T_0 E_0}[\sin(\omega_{rf}\tau + \phi_s) - \sin\phi_s]\frac{\partial}{\partial\delta}$$
$$+ (\omega_\beta + \xi\omega_0\delta)p\frac{\partial}{\partial x} - (\omega_\beta + \xi\omega_0\delta)x\frac{\partial}{\partial p}, \tag{2}$$

$$L_{FP} = \alpha_r\frac{\partial}{\partial\delta}\delta + D_r\frac{\partial^2}{\partial\delta^2}, +\alpha_x\frac{\partial}{\partial p}p + D_x\frac{\partial^2}{\partial p^2}, \tag{3}$$

$$L_C = F_{\tau,m}(\tau, t)\frac{\partial}{\partial\delta} + F_{x,m}(\tau, t)\frac{\partial}{\partial p} \tag{4}$$

and

$$F_{\tau,m}(\tau, t) = -A_\tau \sum_{k=0}^{+\infty}\sum_{m'=0}^{M-1} N_{m'}\int_D d\tau' W_0'(\tau - \tau' + a_{mm'}^k T_0)$$
$$\times \lambda_m'(\tau', t - a_{mm'}^k T_0), \tag{5}$$

$$F_{x,m}(\tau, t) = -A_x \sum_{k=0}^{+\infty}\sum_{m'=0}^{M-1} N_{m'}\int_D d\tau' W_1(\tau - \tau' + a_{mm'}^k T_0)$$
$$\times d_{x,m}(\tau', t - a_{mm'}^k T_0), \tag{6}$$

$$a_{mm'}^k = k + \frac{m - m'}{M}, \tag{7}$$

$$\lambda_m(\tau, t) = \int_{-\infty}^{+\infty} d\delta dx dp\, \Psi_m(\tau, \delta, x, p, t), \tag{8}$$

$$d_{x,m}(\tau, t) = \int_{-\infty}^{+\infty} d\delta dx dp\, x\Psi_m(\tau, \delta, x, p, t), \tag{9}$$

where L_H and L_{FP} are, respectively, the Hamiltonian and Fokker-Planck operators for single particle dynamics, L_C is the collective (effects) operator, with contributions from the longitudinal $F_{\tau,m}$ and transverse $F_{x,m}$ wake forces, and $p = p_x/\omega_\beta$ is the transverse momentum normalized to the betatron frequency ω_β. Here the phase space coordinates (τ, δ, x, p) are arrival time τ, relative energy deviation $\delta = (E - E_0)/E_0$, where E_0 is the energy of the reference

particle in electron volts, transverse position x and transverse momentum p; η is the momentum compaction, T_0 the revolution period, e is the electron charge, V_{rf} the rf voltage, ω_{rf} the angular rf frequency, ϕ_s the synchronous phase, $\omega_0 = 2\pi/T_0$ the angular revolution frequency, ξ the linear chromaticity, and α_τ and D_τ are the longitudinal, and α_x and D_x the transverse, radiation damping and diffusion coefficients; $A_\tau = e\eta/(cT_0 E_0)$, where c is the speed of light, $A_x = ec/(T_0 E_0)$, W_0' is the longitudinal wake function and W_1 is the transverse dipole wake function [23]. In the definition of the wake functions we use the causality condition $W_0'(\tau) = W_1(\tau) = 0$ if $\tau < 0$. $D = [-L/2 : L/2]$ is the region of integration over the longitudinal densities λ_m and $d_{x,m}$; D is therefore assumed to be bounded, with length L shorter than T_0/M. The term with $k = 0$ and $m' = m$ gives the short-range wake force, and the extension of the upper limit of integration to $L/2$ is justified by the causality condition satisfied by the wake functions.

B. Method of solution

To solve the system of Eq. (1) we adopt a splitting method according to the Baker-Campbell-Hausdorff formula,

$$\Psi_m(t + \Delta t) = e^{-(L_H + L_{FP} + L_C)\Delta t}\Psi_m(t)$$
$$= e^{-L_C\Delta t}e^{-L_{FP}\Delta t}e^{-L_H\Delta t}e^{O((\Delta t)^2)}\Psi_m(t), \tag{10}$$

with Δt equal to the revolution period T_0. This is usually a good approximation when the collective force can be treated as a perturbation to the one-turn single particle dynamics. The validity of this approximation can be tested either analytically, by estimating the remainder in the Baker-Campbell-Hausdorff formula, or numerically via simulation convergence studies. Within this approximation, the kick in the particle momentum due to the operator L_C is applied via multiplying the impedance with the average beta function (global impedance) or with the local beta function (local impedance). In case of several local impedances we clump them together and kick the particle momentum according to the sum of the local impedances, each weighted with its own beta function. We therefore update the position of the particles of the mth bunch from turn n to $n + 1$ first by the single particle dynamics operator L_H,

$$\delta_{n+1} = \delta_n + \frac{eV_{rf}}{E_0}[\sin(\omega_{rf}\tau_n + \phi_s) - \sin\phi_s], \tag{11}$$

$$\tau_{n+1} = \tau_n - T_0\eta\delta_{n+1}, \tag{12}$$

$$x_{n+1} = x_n\cos 2\pi(\nu_x + \xi\delta_n) + p_n\sin 2\pi(\nu_x + \xi\delta_n), \tag{13}$$

$$p_{n+1} = -x_n\sin 2\pi(\nu_x + \xi\delta_n) + p_n\cos 2\pi(\nu_x + \xi\delta_n), \tag{14}$$

then by a kick due to the Fokker-Planck operator L_{FP},

$$\delta_{n+1} = \delta_n - \alpha_r T_0 \delta_n + \sqrt{D_r}\zeta_n\sqrt{T_0}, \qquad (15)$$

$$p_{n+1} = p_n - \alpha_x T_0 p_n + \sqrt{D_x}\zeta_n\sqrt{T_0}, \qquad (16)$$

followed by a kick due to the collective operator L_C,

$$\delta_{n+1} = \delta_n + F_{\tau,m}(\tau_n, nT_0)T_0, \qquad (17)$$

$$p_{n+1} = p_n + F_{x,m}(\tau_n, nT_0)T_0, \qquad (18)$$

where, with an abuse of notation, the subscript n is used prior to the update to turn $n+1$ of the following operator. Here ν_x is the betatron tune, and $\zeta(t)$ is a Gaussian white noise $[\langle\zeta(t)\zeta(t')\rangle = 2\delta(t-t')]$ to take into account quantum random excitations.

The parallel algorithm implemented in SPACE to solve Eq. (1) is the following. M bunches, each with the same N_p simulation particles [17] randomly generated according to the initial phase space density, are distributed to M processors. The generation of an arbitrary initial distribution is accomplished with the use of the acceptance-rejection method [24]. At turn n, from the scattered particle positions, the longitudinal density λ_m and the instantaneous transverse dipole density $d_{x,m}$ are constructed on a longitudinal grid $\tau_l = l\Delta$ ($l = 0, \ldots, N_g$, where N_g is the number of grid points and Δ the grid step) of length L with the use of a particle-in-cell deposition scheme. To facilitate the discussion of the algorithms for the computation of the wake forces at $t = nT_0$, we rewrite them in a form to separate the short- and long-range contributions,

$$F_{x,m}(\tau, t) = F_{x,m}^S(\tau, t) + F_{x,n}^L(\tau, t), \qquad (19)$$

where

$$F_{x,m}^S(\tau, t) = -A_x \int_D d\tau' W_1(\tau - \tau') d_{x,m}(\tau', t), \quad (20)$$

$$F_{x,m}^L(\tau, t) = -A_x \sum_{k=0}^{+\infty} \sum_{m'=0}^{M-1} c_{m'k} \int_D d\tau' W_1(\tau - \tau' + a_{mm'}^k T_0)$$
$$\times d_{x,m}(\tau', t - a_{mm'}^k T_0), \qquad (21)$$

and the superscripts S and L indicate the short- and long-range wake forces respectively, and $c_{m'k} = 1 - \delta_{mm'}\delta_{0k}$, where δ_{ij} is the Kronecker delta ($\delta_{ij} = 1$ if $i = j$, 0 otherwise). A similar expression holds for the longitudinal wake force $F_{\tau,m}$.

The parallel algorithm to simulate together short- and long-range wakefield effects consists of a kick given by F^S calculated in serial (locally) by each processor, and a kick from F^L calculated in parallel (globally) via master-to-slave processor communications, by storing the history of moments of the bunches. For dedicated studied of short-range wakefield effects such as high precision simulations

of the microwave instability [14], where a large number of simulation particles is required to study the evolution of microstructures in the bunch, SPACE has the capability to calculate the single-bunch interaction in parallel by distributing the total number of simulation particles between M processors. Parallel algorithms for the calculation of the short-range interaction based on Fourier methods and wavelets, successfully applied to the study of coherent synchrotron radiation in bunch compressors with a two-dimensional Vlasov-Maxwell solver [20,21], are under consideration, as well as algorithms for parallel fast Fourier transform (FFT) calculations.

C. Computation of the short-range wake force

The calculation of the short-range kick F^S uses the FFT method implemented by Blaskiewicz [2] in the TRANFT code, where the application of the convolution theorem allows one to express the Fourier transform of F^S as the product of the Fourier transform of the wake function and the density. For $F_{x,m}^S$, for example, we have

$$\hat{F}_{x,m}^S(\omega, t) = \int_{-\infty}^{\infty} d\tau e^{-i\omega\tau} F_{x,m}^S(\tau, t)$$
$$= iA_x Z_1^\perp(-\omega)\hat{d}_m(\omega, t), \qquad (22)$$

where the following Fourier transform pairs,

$$Z_1^\perp(\omega) = i \int_{-\infty}^{\infty} d\tau e^{i\omega\tau} W_1(\tau), \qquad (23)$$

$$W_1(\tau) = -\frac{i}{2\pi} \int_{-\infty}^{\infty} d\omega e^{-i\omega\tau} Z_1^\perp(\omega), \qquad (24)$$

and

$$\hat{d}_m(\omega, t) = \int_{-\infty}^{\infty} d\tau e^{-i\omega\tau} d_m(\tau, t), \qquad (25)$$

$$d_m(\tau, t) = \frac{1}{2\pi} \int_{-\infty}^{\infty} d\omega e^{i\omega\tau} \hat{d}_m(\omega, t), \qquad (26)$$

hold for the wake function W_1 and the impedance $Z_1^\perp$, and for the transverse dipole density d_m and its transform $\hat{d}_m$. High frequency components of $\hat{F}_{x,m}^S$, induced by numerical noise in the constructed dipole density d_m, can be smoothly suppressed below a cutoff frequency $\omega = \omega_c$ by multiplying $\hat{F}_{x,m}^S$ by an exponential function g with a suitable smoothing parameter α_s,

$$\hat{F}_{x,m}^{S,\text{smooth}}(\omega, t) = \hat{F}_{x,m}^S(\omega, t)e^{-\alpha_s\omega^2}. \qquad (27)$$

By an inverse Fourier transformation, a smooth wake force can be calculated on the longitudinal grid, and the position of the simulation particles updated from a polynomial

interpolation according to their arrival time τ. The Fourier transformations are done efficiently with the use of an FFT. Other than the use of the Fourier method described above, alternative algorithms for noise removal and density estimation from particles are implemented in SPACE, with the goal, besides the calculation of smooth wake forces, to monitor the evolution of distribution densities [21].

1. Computational load

The computational load of the wake force calculation with the FFT is $\mathcal{O}(N_g \log_2 N_g)$, where N_g is the number of points of the longitudinal grid. This should be compared with the computational load of the particle tracking and particle deposition scheme, which is $\mathcal{O}(N_p)$, where N_p is the number of simulation particles.

When comparing the computational load of different algorithms, we would like to point out that only orders of magnitude are meaningful, since the ultimate comparison should rely on computer simulations. This is discussed, for FFT algorithms, in [25], where it is stated that the performance of FFTs is determined by many factors besides pure arithmetic counts or flops (floating-point operations). At the same time, precise estimates of the number of flops required by FFT algorithms are important not only for performance optimization but for a theoretical understanding as well. For a discrete Fourier transform of size $N = 2^m$, the classic "radix-2" FFT algorithm introduced by Cooley and Tukey [26], which is implemented in SPACE, has a number of flops $\sim 5N \log_2 N$. For a discussion of improved FFT algorithms with a lower number of flops see [25], where the result number of flops $\sim 3.8 \log_2 N$ has been achieved with a modified version of the "split-radix" FFT algorithm introduced by Yavne in 1968 [27].

In standard applications, such as bunch lengthening studies below the microwave instability threshold, or studies of the head-tail effects, a typical grid has $N_g = 100$, and with $N_p \geq 10000$ (on average 100 simulation particles per grid cell) the computational load is dominated by the particle tracking. For simulations above the microwave instability threshold, where microstructures in the beam are studied in response to wakefields with high frequency components, a large number of grid points is used, and, consequently, a large number of simulation particles. In such a case the particle tracking and charge deposition are done in parallel by distributing N_p simulation particles between M processors. Assuming simulations with $M = 100$, $N_g = 10000$ and $N_p = 100N_g$, the computational load of the wake force calculation dominates over the computational load of the particle tracking. As an example of the computational load required in the study of the microwave instability, in [14] high resolution simulations with SPACE, with parameters of the NSLS-II storage ring, have been done at NERSC [28] with 15M simulation particles distributed over 1000 processors, with a CPU time of approximately 20 min. To further optimize the

simulations, the use of a parallel FFT can be considered, or the use of wavelets or alternative Fourier methods [20,21].

D. Computation of the long-range wake force

The general algorithm for the calculation of the long-range wake force is as follows. Considering the transverse long-range force $F_{x,n}^L$, for example, given by Eq. (21), we have

$$
\begin{aligned}
F_{x,m}^L(\tau,t) &= -A_x \sum_{k=0}^{k_c} \sum_{m'=0}^{M-1} c_{m'k} \int_D d\tau' W_1(\tau - \tau' + a_{m'm}^k T_0) \\
&\quad \times d_{x,m'}(\tau', t - a_{m'm}^k T_0) \\
&= -A_x \sum_{k=0}^{k_c} \sum_{m'=0}^{M-1} c_{m'k} \int_D d\tau' W_1(\tau - \tau' + a_{m'm}^k T_0) \\
&\quad \times d_{x,m'}(\tau', t - kT_0),
\end{aligned} \tag{28}
$$

where in the last equality we used the approximation $d_{x,m}(\tau, t + T_0) \approx d_{x,m}(\tau, t)$, i.e., we assumed $d_{x,m}$ is slowly varying over one revolution, and we introduced the cutoff k_c in the summation over k determined by the decay rate of W_1. Here we remind that $a_{m'm}^k = k + (m' - m)/M$ and $D = [-L/2; L/2]$, with L the length of the longitudinal grid. If we now assume that the wake function $W_1(\tau)$ is slowly varying for $\tau \in [a_{m'm}^k T_0 - L/2; a_{m'm}^k T_0 + L/2]$, we can conveniently calculate Eq. (28) by expanding W_1 in Taylor series at $a_{m'm}^k T_0$:

$$
\begin{aligned}
F_{x,m}^L(\tau,t) &= -A_x \sum_{k=0}^{k_c} \sum_{m'=0}^{M-1} c_{m'k} \sum_{n=0}^{N_{\mathrm{TL}}} \frac{W_1^{(n)}(a_{m'm}^k T_0)}{n!} \\
&\quad \times \sum_{l=0}^n (-1)^l \binom{n}{l} \tau^{n-l} \langle \tau^l x \rangle_{m'}^k,
\end{aligned} \tag{29}
$$

where $\langle \tau^n x \rangle_m^k = \int d\tau \tau^n d_{x,m}(\tau, t - kT_0)$, N_{TL} is the number of Taylor terms and we made use of the binomial theorem $(a + b)^n = \sum_{k=0}^n \binom{n}{k} a^{n-k} b^k$. The calculation of the wake force $F_{x,m}^L(\tau, t)$ can therefore be done by storing the moments $\langle \tau^n x \rangle_m^k$ of the mth bunch over previous k_c turns. An equation similar to (29) holds for the longitudinal wake force $F_{\tau,m}^L(\tau, t)$ in terms of the stored moments $\langle \tau^n \rangle_m^k = \int d\tau \tau^n \lambda_m(\tau, t - kT_0)$. For point bunch simulations, only the first term in the rhs of Eq. (29) is calculated. Equation (29) requires the evaluation of the N_{TL} derivatives $W_1^{(n)}$ on the longitudinal grid. This can be done upfront, before the beginning of the temporal evolution. In case the wake functions are given numerically as input files, the derivatives $W_1^{(n)}$ can be calculated efficiently with high-order finite difference schemes. As an illustrative example of the application of Eq. (29), in Fig. 1 we discuss the construction of a longitudinal wake function that decays
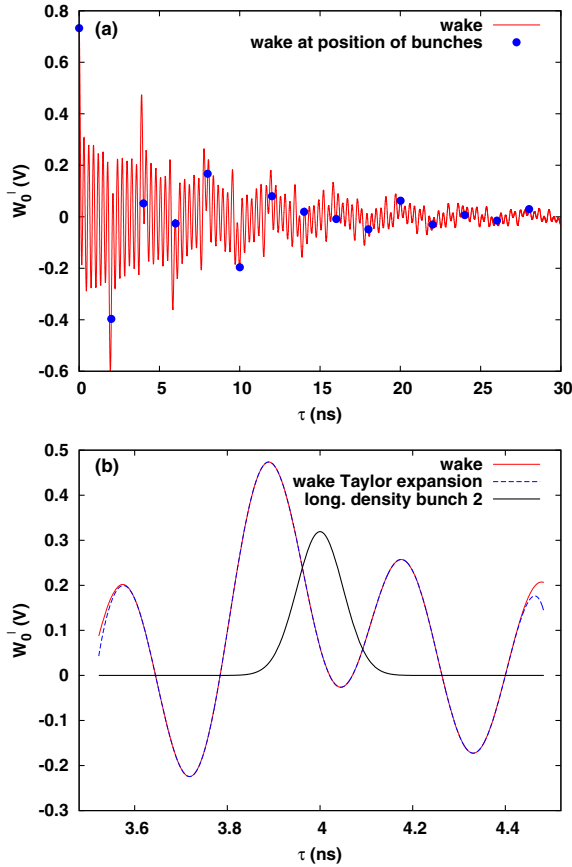
FIG. 1. Construction of the longitudinal wake force from the Taylor expansion of the wake function shown by the red line. (a) The points in blue represent the wake function evaluated at the position of bunches, separated by 2 ns. (b) Reconstruction of the wake function, shown by the dashed blue line, around the centroid of bunch $m = 2$ with 25 terms in the Taylor expansion, necessary for the study of bunch dipole oscillations up to $\pm 10\sigma$, where σ is the bunch length (here $\sigma = 50$ ps).

over less than a revolution period, as shown in Fig. 1(a). Only a fraction of the bunches filling the ring are coupled (here we consider $M = h$ bunches filling uniformly the NSLS-II booster with harmonic number $h = 264$). The wake function shows a large variation over the length σ of the bunches, thus making the wake function reconstruction difficult. This example shows an extreme case, delimiting the transition from short- to long-range interaction. For an accurate reconstruction of the wake function to study, for example, dipole oscillations up to $\pm\sigma$, 25 terms in the Taylor expansion must be calculated, as shown in Fig. 1(b). In such a case one may consider if it is more efficient to calculate directly the wake function without Taylor expanding. A similar expansion of the longitudinal wake function up to few Taylor terms allows one to take into account finite bunch length effects, as discussed in [9] and [15]. This method is general and applicable to arbitrary long-range wakefields. In the case of a resonator wake, the integration over history can be avoided by the use of invariance
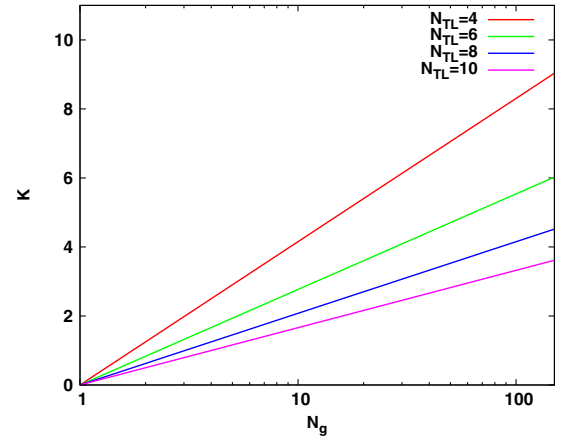

FIG. 2. Comparison of the computational load for the FFT method with the computational load for the method based on Taylor expansion. The ratio of the computational loads $K = 5\log_2 N_g / N_{TL}$ as a function of number of grid points N_g is shown for a different number of Taylor terms N_{TL}.

properties under translation of the resonator wake function [15,29,30]. The idea to express a general wake function as a sum of resonators has been implemented recently by Migliorati *et al.* [1] in the tracking code MuSiC to simulate multibunch effects. The comparison of the computational efficiency of this method with our method based on a Taylor expansion is the subject of a future investigation.

1. Computational load

The integration of Eq. (28) to compute the wake force on the longitudinal grid with N_g grid points requires a computational load of $\mathcal{O}(k_c M N_g \log_2 N_g)$ with the FFT method, to be compared with the computational load given by the application of Eq. (29), which is $\mathcal{O}(k_c M N_{TL} N_g)$, where N_{TL} is the number of terms in the Taylor expansion. Using for the FFT method the number of flops $\sim 5 N_g \log_2 N_g$ we define the ratio of the two computational loads $K = 5\log_2 N_g / N_{TL}$. In Fig. 2 we plot K as a function of N_g for a different number of Taylor terms N_{TL}. In many applications of interest $N_{TL} < 10$ thus $K > 3.5$ with $N_g = 128$.

III. ANALYTICAL TREATMENT OF THE COUPLED-BUNCH INSTABILITY FOR ARBITRARY FILLING PATTERNS

The theory of the coupled-bunch instability for uniform filling patterns is well known and formulas for the complex frequency shifts of oscillation modes are available in the general case of nonzero chromaticity and for finite bunch length [23,30–32]. A complete analysis for arbitrary filling patterns, with formulas for the complex frequency shifts, is not available, despite some effort being put to characterize the coupled-bunch instability in this regime [33–35]. In this

section, we discuss a theoretical treatment of the coupled-bunch instability for arbitrary filling patterns, which leads to the formulation of an eigenvalue problem defined in terms of the complex frequency shifts of the uniform filling pattern case. A similar result, for point bunches and in the longitudinal case, has been derived by Prabhakar [35]. The solution of the eigenvalue problem allows the determination of the eigenvalue with the largest imaginary part, thus characterizing the growth rate of the fastest coupled bunch instability. We restrict our analysis to the dipole mode of oscillation, and to the case of zero chromaticity. The analysis of higher head-tail modes and the discussion of chromaticity effects will be addressed elsewhere [22]. The starting framework of our formulation is defined by the system of M-coupled Vlasov equations defined by Eq. (1), which give the time evolution of the phase space densities Ψ_m associated with the mth bunch. We assume linearized longitudinal equations of motion and neglect quantum radiation effects. For the evolution of the dipole moment, the last assumption has the effect to neglect an exponential decay determined by the radiation damping constant. The equation for the evolution of the dipole moment is found by integrating by parts the Vlasov equations, by using the boundary conditions satisfied by the phase space density Ψ_m, and the eigenvalue problem is formulated with respect to the complex frequency shifts of the uniform filling pattern case.

A. Transverse eigenanalysis

The transverse phase space densities $\Psi_m(\tau, \delta, x, p_x, t)$, associated to the mth bunch with N_m particles, satisfy the following system of M-coupled Vlasov equations for $0 \leq m \leq M-1$:

$$
\frac{\partial \Psi_m}{\partial t} - \eta\delta\frac{\partial \Psi_m}{\partial \tau} + \frac{\omega_s^2}{\eta}\tau\frac{\partial \Psi_m}{\partial \delta} + p_x\frac{\partial \Psi_m}{\partial x} - \omega_\beta^2 x\frac{\partial \Psi_m}{\partial p_x}
$$
$$
- A_x \sum_{k=0}^{+\infty}\sum_{m'=0}^{M-1} N_{m'}\left[\int_{-\infty}^{\tau} d\tau' W_1(\tau - \tau' + a_{m'm}^k T_0)\right.
$$
$$
\left. \times \int_{-\infty}^{+\infty} dx' x' \rho_{m'}(\tau', x', t - a_{m'm}^k T_0)\right]\frac{\partial \Psi_m}{\partial p_x} = 0, \qquad (30)
$$

where $a_{m'm}^k = k + \frac{m'-m}{M}$ and

$$
\rho_m(\tau, x, t) = \int_{-\infty}^{+\infty}\int_{-\infty}^{+\infty} d\delta dp_x \Psi_m(\tau, \delta, x, p_x, t),
$$

$\eta = \alpha - 1/\gamma^2$ is the slippage factor, α is the momentum compaction factor, and ω_s the synchrotron frequency, W_1 is the transverse wake function, and $\sum_{m=0}^{M-1} N_m = NM = N_T$ is the total number of particles in the filling pattern, with N the number of particles per bunch in the uniform filling pattern case. We neglect longitudinal wakefields, so for the longitudinal equations of motion we consider $\dot{\tau} = -\eta\delta$,

$\dot{\delta} = \omega_s^2 \tau/\eta$, $\dot{} \equiv d/dt$. The equation for the evolution of the dipole moments $\langle x_m\rangle = \int d\tau d\delta dx dp_x x \Psi_m$ and $\langle p_{x_m}\rangle = \int d\tau d\delta dx dp_x p_x \Psi_m$ can be found by integrating by parts the Vlasov equations using the boundary conditions for Ψ_m. Multiplying the Vlasov equation by x and integrating we obtain

$$
\frac{d}{dt}\langle x_m\rangle = \int_{-\infty}^{+\infty} d\tau d\delta dx dp_x x\frac{\partial \Psi_m}{\partial t}
$$
$$
= -\int_{-\infty}^{+\infty} d\tau d\delta dp_x p_x\left(x\Psi_m|_{x=-\infty}^{x=+\infty} - \int_{-\infty}^{+\infty} dx\Psi_m\right)
$$
$$
= \langle p_{x_m}\rangle. \qquad (31)
$$

For $\langle p_{x_m}\rangle$ we proceed similarly obtaining the result

$$
\frac{d^2}{dt^2}\langle x_m\rangle + \omega_\beta^2\langle x_m\rangle
$$
$$
= -A_x \sum_{k=0}^{+\infty}\sum_{m'=0}^{M-1} N_{m'}
$$
$$
\times \int_{-\infty}^{+\infty} d\tau \int_{-\infty}^{+\infty} d\tau' W_1(\tau - \tau' + a_{m'm}^k T_0)\lambda_m(\tau, t)
$$
$$
\times \int_{-\infty}^{+\infty} dx' x' \rho_{m'}(\tau', x', t - a_{m'm}^k T_0), \qquad (32)
$$

where $\lambda_m(\tau, t) = \int dx\rho_m(\tau, x, t)$ is the longitudinal distribution density of the mth bunch, and we have extended the upper limit of integration in τ' to $+\infty$, due to the causality property of W_1. Using the approximation $\rho_m(\tau, x, t) = \lambda(\tau)\mu_m(x, t)$ in the rhs of Eq. (32), where $\mu_m(x, t) = \int d\tau\rho_m(\tau, x, t)$ is the transverse distribution density of the mth bunch, we have

$$
\frac{d^2}{dt^2}\langle x_m\rangle + \omega_\beta^2\langle x_m\rangle = -A_x \sum_{k=0}^{+\infty}\sum_{m'=0}^{M-1} f(a_{m'm}^k T_0)
$$
$$
\times N_{m'}\langle x_{m'}\rangle(t - a_{m'm}^k T_0), \qquad (33)
$$

where

$$
f(x) \equiv \int_{-\infty}^{+\infty} d\tau \int_{-\infty}^{+\infty} d\tau' W_1(\tau - \tau' + x)\lambda(\tau)\lambda(\tau').
$$

Clearly in the point bunch limit $\lambda(\tau) = \delta(\tau)$, where δ is the Dirac delta function, and $f(x) = W_1(x)$, the equations for point bunches are recovered.

We proceed now by omitting the brackets in the equations, i.e., x_m should be understood as $\langle x_m\rangle$. We notice that the equations of motion, Eq. (33), can be cast in the form

$$\ddot{x}_m(t) + \omega_\beta^2 x_m(t) = -A_x \sum_{k=0}^{+\infty} f\left(k\frac{T_0}{M}\right) N_{[m+k]} x_{[m+k]}$$
$$\times \left(t - k\frac{T_0}{M}\right), \qquad (34)$$

where $[m+k] = m + k - M\lfloor (m+k)/M \rfloor$. Here $\lfloor x \rfloor$ is the floor function, also called greatest integer value, which gives the largest integer less or equal to x [36]. Defining the mode $\tilde{x}_\mu$ by

$$\tilde{x}_\mu(t) = \sum_{m=0}^{M-1} x_m(t) e^{-i2\pi m\mu/M}, \qquad (35)$$

$$x_m(t) = \frac{1}{M} \sum_{\mu=0}^{M-1} \tilde{x}_\mu(t) e^{i2\pi m\mu/M}, \qquad (36)$$

it follows that the modes $\tilde{x}_\mu$ are coupled and satisfy the equations of motion,

$$\ddot{\tilde{x}}_\mu(t) + \omega_\beta^2 \tilde{x}_\mu(t) = -\frac{A_x}{M} \sum_{k=0}^{\infty} f\left(k\frac{T_0}{M}\right) e^{i2\pi\mu k/M}$$
$$\times \sum_{\mu'=0}^{M-1} \tilde{x}_{\mu'}\left(t - k\frac{T_0}{M}\right)$$
$$\times \sum_{m=0}^{M-1} N_m e^{i2\pi m(\mu'-\mu)/M}. \qquad (37)$$

The proof of Eq. (37) is given in Appendix A. By using $\sum_{m=0}^{M-1} = NM$, Eq. (37) can be equivalently written as

$$\ddot{\tilde{x}}_\mu(t) + \omega_\beta^2 \tilde{x}_\mu(t) = -A_x N \sum_{k=0}^{\infty} f\left(k\frac{T_0}{M}\right) e^{i2\pi k\mu/M} \tilde{x}_\mu\left(t - k\frac{T_0}{M}\right)$$
$$-\frac{A_x}{M} \sum_{k=0}^{\infty} f\left(k\frac{T_0}{M}\right) e^{i2\pi\mu k/M}$$
$$\times \sum_{\substack{\mu'=0 \\ \mu'\neq\mu}}^{M-1} \tilde{x}_{\mu'}\left(t - k\frac{T_0}{M}\right)$$
$$\times \sum_{m=0}^{M-1} N_m e^{i2\pi m(\mu'-\mu)/M}. \qquad (38)$$

In the uniform filling pattern case, $N_m = N$ and the second term in the rhs of Eq. (38) vanishes, as follows from the orthogonality condition,

$$\sum_{m=0}^{M-1} e^{i2\pi m(\mu'-\mu)/M} = M\delta_{\mu'\mu}, \qquad (39)$$

where $\delta_{\mu'\mu}$ is the Kronecker delta. Thus in the uniform filling pattern case the modes $\tilde{x}_\mu$ are uncoupled.

1. Eigenvalue problem

The general solution of the noncollective equations of motion $\ddot{\tilde{x}}_\mu(t) + \omega_\beta^2 \tilde{x}_\mu(t) = 0$ is

$$\tilde{x}_\mu(t) = A_1 e^{i\omega_\beta t} + A_2 e^{-i\omega_\beta t} = \frac{1}{2}\left[\left(\tilde{x}_\mu(0) - \frac{i}{\omega_\beta}\dot{\tilde{x}}_\mu(0)\right)e^{i\omega_\beta t}\right.$$
$$\left. + \left(\tilde{x}_\mu(0) + \frac{i}{\omega_\beta}\dot{\tilde{x}}_\mu(0)\right)e^{-i\omega_\beta t}\right]. \qquad (40)$$

Since $x_m \in \mathbb{R}$, it follows that $\tilde{x}_\mu = \tilde{x}_{M-\mu}^\star$, thus we define the multibunch mode

$$x_m^{(\mu)}(t) = \frac{1}{M}[\tilde{x}_\mu(t) e^{i2\pi m\mu/M} + \tilde{x}_{M-\mu}(t) e^{-i2\pi m\mu/M}]$$
$$= \frac{1}{M}[\tilde{x}_\mu(t) e^{i2\pi m\mu/M} + \tilde{x}_\mu^\star(t) e^{-i2\pi m\mu/M}]$$
$$= \frac{2}{M}\left(\mathrm{Re}\tilde{x}_\mu(t) \cos\frac{2\pi\mu m}{M} - \mathrm{Im}\tilde{x}_\mu(t) \sin\frac{2\pi\mu m}{M}\right). \qquad (41)$$

We now look for a perturbative solution of Eq. (37), where we identify the perturbation by multiplying the rhs of Eq. (37) with the parameter ϵ. Without loss of generality, we assume for the perturbative solution the form

$$\tilde{x}_\mu(t) = A_1 e^{i(\omega_\beta+\epsilon\Omega)t} + A_2 e^{-i(\omega_\beta+\epsilon\Omega)t}$$
$$= a_\mu e^{-i(\omega_\beta+\epsilon\Omega)t}, \qquad \Omega \in \mathbb{C}, \qquad (42)$$

where $a_\mu = \tilde{x}_\mu(0)$ and we chose $A_1 = 0$. Defining $\tau^{-1} \equiv \mathrm{Im}\Omega$, $\omega_r \equiv \mathrm{Re}\Omega$ and assuming $\mathrm{Im}\tilde{x}_\mu(0) = 0$, the multibunch mode $x_m^{(\mu)}$ takes the form

$$x_m^{(\mu)}(t) = a e^{\frac{t}{\tau}}\left(\cos\frac{2\pi\mu m}{M}\cos(\omega_\beta + \omega_r)t\right.$$
$$\left. + \sin\frac{2\pi\mu m}{M}\sin(\omega_\beta + \omega_r)t\right), \qquad (43)$$

where $a = 2\mathrm{Re}\tilde{x}_\mu(0)/M$ and we set the perturbation parameter $\epsilon = 1$.

By inserting Eq. (42) in Eq. (37) we obtain, to first order in ϵ,

$$\Omega a_\mu = \frac{A_x}{2\omega_\beta M} \sum_{\mu'=0}^{M-1} a_{\mu'} \sum_{k=0}^{\infty} f\left(k\frac{T_0}{M}\right) e^{i2\pi\mu k/M} e^{i\omega_\beta kT_0/M}$$
$$\times \sum_{m=0}^{M-1} N_m e^{i2\pi m(\mu'-\mu)/M}. \qquad (44)$$

Using Eq. (38), we can rewrite Eq. (44) in the form

$$\left[\frac{A_x N}{2\omega_\beta}\sum_{k=0}^{\infty} f\left(k\frac{T_0}{M}\right)e^{i2\pi\mu k/M}e^{i\omega_\beta kT_0/M}-\Omega\right]a_\mu$$

$$+\sum_{\substack{\mu'=0\\\mu'\neq\mu}}^{M-1}\left[\frac{A_x}{2\omega_\beta M}\sum_{k=0}^{\infty} f\left(k\frac{T_0}{M}\right)e^{i2\pi\mu k/M}e^{i\omega_\beta kT_0/M}\right.$$

$$\left.\times\sum_{m=0}^{M-1}N_m e^{i2\pi m(\mu'-\mu)/M}\right]a_{\mu'}=0. \qquad (45)$$

Equation (45) defines an eigenvalue equation for the matrix $\mathbf{B}$:

$$(\mathbf{B}-\Omega\mathbf{I})\mathbf{a}=0,$$

$$B_{\mu\mu'}=\frac{\Omega_\mu^U}{NM}\sum_{m=0}^{M-1}N_m e^{i2\pi m(\mu'-\mu)/M},$$

$$\mathbf{a}=[a_0,\dots,a_{M-1}]^T, \qquad (46)$$

where Ω_μ^U are the eigenvalues of the uniform filling pattern case ($B_{\mu\mu'}=\Omega_\mu^U$ if $\mu'=\mu$, 0 otherwise) and are given by (see Appendix B)

$$\Omega_\mu^U=\frac{A_x N}{2\omega_\beta}\sum_{k=0}^{\infty} f\left(k\frac{T_0}{M}\right)e^{i2\pi\mu k/M}e^{i\omega_\beta kT_0/M}$$

$$=-i\frac{I_b Mc}{4\pi(E_0/e)\nu_\beta}\sum_{p=-\infty}^{+\infty}|\tilde{\lambda}(pM\omega_0+\mu\omega_0+\omega_\beta)|^2$$

$$\times Z_1^\perp[pM\omega_0+\mu\omega_0+\omega_\beta], \qquad (47)$$

where $I_b=eN/T_0$ and $\nu_\beta=\omega_\beta/\omega_0$. Solving for the characteristic polynomial $p(\Omega)=|\mathbf{B}-\Omega\mathbf{I}|=0$ and assuming M distinct eigenvalues Ω_m, the general solution $\tilde{x}_\mu^g(t)$ is given by[1]

$$\tilde{x}_\mu^g(t)=\sum_{m=0}^{M-1}c_m a_{\mu m}e^{-i(\omega_\beta+\Omega_m)t}, \qquad (48)$$

where $\mathbf{a}_m=[a_{0m},\dots,a_{M-1m}]^T$ are the eigenvectors associated to the eigenvalues Ω_m. Since the sum of the eigenvalues of $\mathbf{B}$ is equal to the trace of $\mathbf{B}$, it follows that the sum of the complex frequency shifts Ω_μ for arbitrary filling patterns is equal to the sum of the complex frequency shifts Ω_μ^U for uniform filling patterns,

---

[1]In deriving Eq. (44) we considered only one root of Eq. (37). To construct the complete solution, in Eq. (48) a term proportional to $\exp i(\omega_\beta+\Omega_m)t$ should be added. This is important to explicitly study the modes of oscillations defined by the solution of the eigenvalue problem. In the present work we limit our analysis to the characterization of the eigenvalue spectrum, and will investigate the modes of oscillations in a separate companion paper.

$$\sum_{\mu=0}^{M-1}\Omega_\mu=\mathrm{Tr}\,\mathbf{B}\Rightarrow\sum_{\mu=0}^{M-1}\Omega_\mu=\sum_{\mu=0}^{M-1}\Omega_\mu^U. \qquad (49)$$

B. Longitudinal eigenanalysis

In the longitudinal case we use path length s as independent variable and $'\equiv d/ds$, and as phase space coordinates we use (z,δ), where $z=\beta_r c\tau$, with $\beta_r=v_r/c$ and v_r is the velocity of the reference particle. Here we assume $\beta_r=1$. The set of M-coupled Vlasov equations satisfied by the phase space densities $g_m(z,\delta,s)$ reads

$$\frac{\partial g_m}{\partial s}-\eta\delta\frac{\partial g_m}{\partial z}+\frac{\omega_s^2}{\eta c^2}z\frac{\partial g_m}{\partial\delta}-A_z\sum_{k=0}^{+\infty}\sum_{m'=0}^{M-1}N_{m'}$$

$$\times\int_{-\infty}^{z}dz'W_0'(z-z'+a_{m'm}^k C)$$

$$\times\lambda_{m'}(z',s-a_{m'm}^k C)\frac{\partial g_m}{\partial\delta}=0, \qquad (50)$$

where $a_{m'm}^k=k+\frac{m'-m}{M}$ and $\lambda_m(z,s)=\int_{-\infty}^{+\infty}d\delta g_m(z,\delta,s)$, and $A_z=e\eta/(cT_0 E_0)$. As in the transverse case we neglect radiation damping and diffusion. The equation for the evolution of the dipole moments $\langle z_m\rangle=\int dz d\delta z g_m(z,\delta,s)$ and $\langle\delta_m\rangle=\int dz d\delta\delta g_m(z,\delta,s)$ can be found by integrating by parts the Vlasov equations using the boundary conditions for g_m. Multiplying the Vlasov equations by z and integrating we obtain

$$\frac{d}{ds}\langle z_m\rangle=\int_{-\infty}^{+\infty}dz d\delta z\frac{\partial g_m}{\partial s}$$

$$=\eta\int_{-\infty}^{+\infty}dz d\delta\,\delta\left(zg_m|_{z=-\infty}^{z=+\infty}-\int_{-\infty}^{+\infty}dz g_m\right)$$

$$=-\eta\langle\delta_m\rangle, \qquad (51)$$

where we assume that the longitudinal phase space densities have a finite integration range in z, much shorter than the distance between bunches $d=C/M$. For $\langle\delta_m\rangle$ we proceed similarly obtaining the result

$$\frac{d^2}{ds^2}\langle z_m\rangle+\frac{\omega_s^2}{c^2}\langle z_m\rangle=-A_z\sum_{k=0}^{+\infty}\sum_{m'=0}^{M-1}N_{m'}\int_{-\infty}^{+\infty}dz$$

$$\times\int_{-\infty}^{+\infty}dz'W_0'(z-z'+a_{m'm}^k C)$$

$$\times\lambda_m(z,s)\lambda_{m'}(z',s-a_{m'm}^k C), \qquad (52)$$

where we have extended the upper limit of integration in z' to $+\infty$, due to the causality property of W_0'. We now assume small rigid dipole oscillations

$$\lambda_m(z,s)=\lambda_0[z-\langle z_m\rangle(s)] \qquad (53)$$

for a given initial distribution $\lambda_0(z)$. It follows that Eq. (52) reads

$$\frac{d^2}{ds^2}\langle z_m\rangle + \frac{\omega_s^2}{c^2}\langle z_m\rangle = -A_z \sum_{k=0}^{+\infty}\sum_{m'=0}^{M-1} N_{m'} \int_{-\infty}^{+\infty} dz \int_{-\infty}^{+\infty} dz' W_0'(z - z' + a_{m'm}^k C)\lambda_0[z - \langle z_m\rangle(s)]$$
$$\times \lambda_0[z' - \langle z_{m'}\rangle(s - a_{m'm}^k C)]. \tag{54}$$

Changing integration variable $u = z' - \langle z_{m'}\rangle(s - a_{m'm}^k C)$, Eq. (54) reads

$$\frac{d^2}{ds^2}\langle z_m\rangle + \frac{\omega_s^2}{c^2}\langle z_m\rangle = -A_z \sum_{k=0}^{+\infty}\sum_{m'=0}^{M-1} N_{m'} \int_{-\infty}^{+\infty} dz \int_{-\infty}^{+\infty} du W_0'[z - \langle z_{m'}\rangle(s - a_{m'm}^k C) + a_{m'm}^k C - u]\lambda_0[z - \langle z_m\rangle(s)]\lambda_0(u) \tag{55}$$

Expanding next W_0' in Taylor series for small $\langle z_{m'}\rangle$ we have

$$\frac{d^2}{ds^2}\langle z_m\rangle + \frac{\omega_s^2}{c^2}\langle z_m\rangle = -A_z \sum_{k=0}^{+\infty}\sum_{m'=0}^{M-1} N_{m'} \int_{-\infty}^{+\infty} dz \int_{-\infty}^{+\infty} du W_0'(z + a_{m'm}^k C - u)\lambda_0[z - \langle z_m\rangle(s)]\lambda_0(u)$$
$$+ A_z \sum_{k=0}^{+\infty}\sum_{m'=0}^{M-1} N_{m'} \int_{-\infty}^{+\infty} dz \int_{-\infty}^{+\infty} du W_0''(z + a_{m'm}^k C - u)$$
$$\times \lambda_0[z - \langle z_m\rangle(s)]\lambda_0(u)\langle z_{m'}\rangle(s - a_{m'm}^k C) + \cdots. \tag{56}$$

The first term in the rhs of Eq. (56) gives a static term that leads to a synchronous phase shift, and a dynamic term that leads to a synchrotron frequency shift. To show it, by changing integration variable $v = z - \langle z_m\rangle(s)$ and expanding in Taylor series for small $\langle z_m\rangle$ we have

$$-A_z \sum_{k=0}^{+\infty}\sum_{m'=0}^{M-1} N_{m'} \int_{-\infty}^{+\infty} dv \int_{-\infty}^{+\infty} du W_0'[v + \langle z_m\rangle(s) + a_{m'm}^k C - u] \times \lambda_0(v)\lambda_0(u)$$
$$= -A_z \sum_{k=0}^{+\infty}\sum_{m'=0}^{M-1} N_{m'} \int_{-\infty}^{+\infty} dv \int_{-\infty}^{+\infty} du W_0'(v + a_{m'm}^k C - u)\lambda_0(v)\lambda_0(u)$$
$$- A_z \sum_{k=0}^{+\infty}\sum_{m'=0}^{M-1} N_{m'} \int_{-\infty}^{+\infty} dv \int_{-\infty}^{+\infty} du W_0''(v + a_{m'm}^k C - u)\lambda_0(v)\lambda_0(u)\langle z_m\rangle(s) + \cdots. \tag{57}$$

With the same change of integration variable applied to the second term in the rhs of Eq. (56), and by dropping the static term [first term in the rhs of Eq. (57)], it follows that Eq. (56), to leading order in $\langle z_m\rangle$ reads

$$\frac{d^2}{ds^2}\langle z_m\rangle + \frac{\omega_s^2}{c^2}\langle z_m\rangle = A_z \sum_{k=0}^{+\infty}\sum_{m'=0}^{M-1} N_{m'} h(a_{m'm}^k C)\langle z_{m'}\rangle(s - a_{m'm}^k C), \tag{58}$$

where $h(x) \equiv \int dz \int dz' W_0''(z - z' + x)\lambda_0(z)\lambda_0(z')$ and the synchrotron frequency ω_s has been redefined according to

$$\omega_s^2 \to \omega_s^2 - A_z c^2 \sum_{k=0}^{+\infty}\sum_{m'=0}^{M-1} N_{m'} h(a_{m'm}^k C). \tag{59}$$

Clearly in the point bunch limit $\lambda(z) = \delta(z)$ and $h(z) = W_0''(z)$, and the equations of motion for point bunches are recovered.

Similarly to the transverse case, we proceed by omitting the brackets in the equations of motion, i.e., z_m should be understood as $\langle z_m\rangle$, and cast the equations of motion (58) in the form

$$z_m''(s) + \left(\frac{\omega_s}{c}\right)^2 z_m(s) = A_z \sum_{k=0}^{+\infty} h\left(k\frac{C}{M}\right) N_{[m+k]} z_{[m+k]}\left(s - k\frac{C}{M}\right),$$

where $[m + k] = m + k - M\lfloor (m + k)/M \rfloor$. Defining the mode $\tilde{z}_\mu$ by

$$
\tilde{z}_\mu(s) = \sum_{m=0}^{M-1} z_m(s) e^{-i2\pi m\mu/M},
$$

$$
z_m(s) = \frac{1}{M} \sum_{\mu=0}^{M-1} \tilde{z}_\mu(s) e^{i2\pi m\mu/M},
\tag{60}
$$

the modes $\tilde{z}_\mu$ are coupled and satisfy the equations of motion

$$
\tilde{z}_\mu''(s) + \frac{\omega_s^2}{c^2} \tilde{z}_\mu(s) = \frac{A_z}{M} \sum_{k=0}^{\infty} h\left(k\frac{C}{M}\right) e^{i2\pi\mu k/M} \sum_{\mu'=0}^{M-1} \tilde{z}_{\mu'}\left(s - k\frac{C}{M}\right) \sum_{m=0}^{M-1} N_m e^{i2\pi m(\mu'-\mu)/M}.
\tag{61}
$$

The proof of Eq. (61) is analogous to the proof of Eq. (37) given in Appendix B. As in the transverse case, by using $\sum_{m=0}^{M-1} = NM$, Eq. (61) can be equivalently written as

$$
\tilde{z}_\mu''(s) + \frac{\omega_s^2}{c^2} \tilde{z}_\mu(s) = A_z N \sum_{k=0}^{\infty} h\left(-k\frac{C}{M}\right) e^{i2\pi k\mu/M} \tilde{z}_\mu\left(s - k\frac{C}{M}\right) + \frac{A_z}{M} \sum_{k=0}^{\infty} h\left(k\frac{C}{M}\right) e^{i2\pi\mu k/M}
$$

$$
\times \sum_{\substack{\mu'=0 \\ \mu' \neq \mu}}^{M-1} \tilde{z}_{\mu'}\left(s - k\frac{C}{M}\right) \sum_{m=0}^{M-1} N_m e^{i2\pi m(\mu'-\mu)/M},
\tag{62}
$$

and in the uniform filling pattern case $N_m = N$ the second term in the rhs of Eq. (62) vanishes, as follows from the orthogonality condition given by Eq. (39), implying that the modes $\tilde{z}_\mu$ are uncoupled.

1. Eigenvalue problem

The eigenvalue problem for the longitudinal case is defined as in the transverse case. We look for a perturbative solution of Eq. (61), where we identify the perturbation by multiplying the rhs of Eq. (61) with the parameter ϵ. We assume the perturbative solution has the form

$$
\tilde{z}_\mu(s) = a_\mu e^{-i(\omega_s + \epsilon\Omega)\frac{s}{c}}, \qquad \Omega \in \mathbb{C}.
\tag{63}
$$

By inserting Eq. (63) in Eq. (61) we obtain, to first order in ϵ,

$$
\Omega a_\mu = -\frac{A_z c^2}{2\omega_s M} \sum_{\mu'=0}^{M-1} a_{\mu'} \sum_{k=0}^{\infty} f\left(-k\frac{C}{M}\right) e^{i2\pi\mu k/M} e^{i\omega_s kT_0/M} \sum_{m=0}^{M-1} N_m e^{i2\pi m(\mu'-\mu)/M}.
\tag{64}
$$

Using Eq. (62), we can rewrite Eq. (64) in the form

$$
\left[-\frac{A_z N c^2}{2\omega_s} \sum_{k=0}^{\infty} h\left(k\frac{C}{M}\right) e^{i2\pi\mu k/M} e^{i\omega_s kT_0/M} - \Omega \right] a_\mu + \sum_{\substack{\mu'=0 \\ \mu' \neq \mu}}^{M-1} \left[-\frac{A_z c^2}{2\omega_s M} \sum_{k=0}^{\infty} h\left(k\frac{C}{M}\right) e^{i2\pi\mu k/M} e^{i\omega_s kT_0/M} \right.
$$

$$
\left. \times \sum_{m=0}^{M-1} N_m e^{i2\pi m(\mu'-\mu)/M} \right] a_{\mu'} = 0.
\tag{65}
$$

Equation (65) defines an eigenvalue equation for the matrix **D**

$$(\mathbf{D} - \Omega \mathbf{I})\mathbf{a} = 0,$$

$$D_{\mu\mu'} = \frac{\Omega_\mu^U}{NM} \sum_{m=0}^{M-1} N_m e^{i2\pi m(\mu'-\mu)/M},$$

$$\mathbf{a} = [a_0, ..., a_{M-1}]^T, \qquad (66)$$

where Ω_μ^U are the eigenvalues of the uniform filling pattern case ($D_{\mu\mu'} = \Omega_\mu^U$ if $\mu' = \mu$, 0 otherwise) and are given by (see Appendix B)

$$\Omega_\mu^U = -\frac{A_z Nc^2}{2\omega_s} \sum_{k=0}^{\infty} h\left(k\frac{C}{M}\right) e^{i2\pi\mu k/M} e^{i\omega_s kT_0/M} \qquad (67)$$

$$= i \frac{I_b M\eta}{4\pi(E_0/e)\nu_s} \sum_{p=-\infty}^{+\infty} (pM\omega_0 + \mu\omega_0 + \omega_s)$$

$$\times |\tilde{\lambda}(pM\omega_0 + \mu\omega_0 + \omega_s)|^2 Z_0^\parallel(pM\omega_0 + \mu\omega_0 + \omega_s), \qquad (68)$$

where $I_b = eN/T_0$ and $\nu_s = \omega_s/\omega_0$. Solving for the characteristic polynomial $p(\Omega) = |\mathbf{D} - \Omega\mathbf{I}| = 0$ and assuming M distinct eigenvalues Ω_m, the general solution $\tilde{z}_\mu^g(s)$ is given by

$$\tilde{z}_\mu^g(s) = \sum_{m=0}^{M-1} c_m a_{\mu m} e^{-i(\omega_s + \Omega_m)\frac{s}{c}}, \qquad (69)$$

where $\mathbf{a}_m = [a_{0m}, ..., a_{M-1 m}]^T$ are the eigenvectors associated to the eigenvalues Ω_m. Since the diagonal terms of $\mathbf{D}$ are the eigenvalues of the uniform filling pattern case, as in the transverse case, the same property given by Eq. (49) holds for the eigenvalues of $\mathbf{D}$:

$$\sum_{\mu=0}^{M-1} \Omega_\mu = \mathbf{Tr}\,\mathbf{D} \Rightarrow \sum_{\mu=0}^{M-1} \Omega_\mu = \sum_{\mu=0}^{M-1} \Omega_\mu^U. \qquad (70)$$

IV. APPLICATION OF THE EIGENVALUE FORMULATION FOR ARBITRARY FILLING PATTERN

A. Benchmarking theory and simulations

To validate the analysis of the coupled bunch instability for arbitrary filling patterns discussed in the previous section, we benchmark the solution of the eigenvalue equation (46) against SPACE simulations, with the parameter of the transverse coupled bunch instability driven by the HOMs of a seven-cell PETRA-III rf cavity discussed in [11], where a detailed benchmark of SPACE simulations against the analytical theory for uniform filling patterns can be found. The parameters of the NSLS-II storage ring are listed in Table I and HOMs parameters in Table II. As

TABLE I. Parameters for NSLS-II bare lattice.

Parameter	Symbol	Value	Unit
Energy	E_0	3	GeV
Revolution period	T_0	2.64	μs
Harmonic number	h	1320	
Average current[a]	I_{av}	25	mA
Momentum compaction	α	0.00037	
Synchrotron tune	ν_s	0.007	
Horizontal tune	ν_x	33.22	
Vertical tune	ν_y	16.26	
Transverse damping time	$\tau_{x,y}$	54	ms
Longitudinal damping time	τ_s	27	ms
Energy spread	σ_δ	0.0005	
Bunch length	σ_t	10	ps

[a]Commissioning stage up to 25 mA.

discussed in the previous sections, with M we represent the number of bunches filling the ring uniformly. The number of possible uniform configurations is determined by the harmonic number h, which corresponds to the total number of rf buckets. For the NSLS-II storage ring, as shown in Table I, $h = 1320 = 2^3 \times 3 \times 5 \times 11$, with the prime factorization determining the possible uniform configurations, thus the possible values of M. A given M determines therefore the number of rf buckets filled, with arbitrary multibunch configurations defined by the number of particles per bunch (per rf bucket) N_m satisfying $\sum_{m=0}^{M-1} N_m = NM$, where $N = N_T/M$ is the number of particles per bunch in the uniform filling pattern case and N_T is the total number of particles in the beam. Of course configurations with missing bunches can be created by filling the mth rf bucket with $N_m = 0$. The cases of two and three bunches ($M = 2$ and $M = 3$) are discussed analytically, with the case of $M = 2$ solved for an arbitrary number of particles per bunch N_0, N_1, and the case of $M = 3$ solved for $N_0 = N_1 = 3N/2$, $N_2 = 0$, thus describing a configuration with a missing bunch. For an arbitrary number of bunches M, the eigenvalue problem is solved numerically. The numerical growth rates are found by fitting with an exponential the envelope of the betatron

TABLE II. Transverse HOMs of the seven-cell PETRA-III rf cavity.

f_r, MHz	$R_{sh,\perp}$, MΩ/m	$Q_\perp$	$R_{sh,\perp}/Q_\perp$, Ω/m
860.25	14.7	55 700	263.91
867.12	17.5	56 800	308.1
869.55	56.1	58 200	963.92
870.96	19.7	59 400	331.65
1043.53	83.6	40 400	2069.31
1047.44	26.2	40 900	640.59
1089.13	17.0	49 400	344.13
1465.13	15.5	54 600	283.88
1545.34	26.8	44 300	604.97

oscillations of the bunch centroids. From the definition of the multibunch mode $x_m^{(\mu)}(t)$ given in Eq. (41), it follows that an arbitrary multibunch configuration can be expressed as a sum of multibunch modes

$$x_m(t) = \frac{1}{2} \sum_{\mu=0}^{M-1} x_m^{(\mu)}(t). \quad (71)$$

In the uniform filling pattern case, the modes x_μ are uncoupled and the multibunch $x_m^{(\mu)}(t)$ is determined by the real and imaginary parts of x_μ:

$$x_m^{(\mu)}(t) = \frac{2}{M} \left(\text{Re}\tilde{x}_\mu(t) \cos\frac{2\pi\mu m}{M} - \text{Im}\tilde{x}_\mu(t) \sin\frac{2\pi\mu m}{M} \right). \quad (72)$$

We therefore calculate the growth rate of mode x_μ via configuring the initial state in the multibunch $x_m^{(\mu)}(t)$. In the arbitrary filling pattern case, the modes x_μ are coupled and their expression is given by Eq. (48). All modes are affected by the eigenvalue with the largest imaginary part, with the degree of coupling given by the initial conditions determined by the eigenvectors. Our procedure to the determine the growth rate in such a case consists of calculating the time evolution x_μ for $\mu = 0, \ldots, M - 1$. After a transient, the exponential increase determined by the eigenvalue with the largest imaginary part becomes dominant, and allows the calculation of the numerical growth rate by exponential fitting. The analysis of the independent modes of oscillation can be done via transforming to the coordinate system defined by the eigenvectors. A detailed investigation of the modes of oscillation for arbitrary filling patterns will be the subject of a future publication. The effect of a gap g in the uniform filling pattern case is studied for $M = h = 1320$, where the number of bunches in the nonuniform filling pattern is $M_g = M - g$, and the number of particles per bunch is $N_g = NM = N_T/M_g$. We show that the imaginary part of the fastest eigenvalue (with the largest positive imaginary part) is very close to the growth rate of the fastest unstable mode of the uniform filling pattern case, over a large range of the gap g.

1. Elementary case 1: Two bunches

For $M = 2$, and with $2N = N_T$, the eigenvalue problem given by Eq. (46),

$$\begin{vmatrix} \Omega_0^U - \Omega & N_- \Omega_0^U \\ N_- \Omega_1^U & \Omega_1^U - \Omega \end{vmatrix} = 0, \qquad N_- = \frac{N_0 - N_1}{N_0 + N_1},$$

$$N_0 + N_1 = 2N,$$

is easily solved, with eigenvalues

$$\Omega_{0,1} = \frac{\Omega_0^U + \Omega_1^U}{2} \pm \frac{1}{2} \sqrt{(\Omega_0^U - \Omega_1^U)^2 + 4N_-^2 \Omega_0^U \Omega_1^U}, \quad (73)$$

$$\Omega_0 + \Omega_1 = \Omega_0^U + \Omega_1^U, \quad (74)$$

and corresponding eigenvectors

$$\mathbf{a}_0 = \left[1, -\frac{2\Omega_1^U N_-}{\Omega_1^U - \Omega_0^U - \sqrt{(\Omega_0^U - \Omega_1^U)^2 + 4N_-^2 \Omega_0^U \Omega_1^U}} \right]^T$$

$$\mathbf{a}_1 = \left[\frac{2\Omega_0^U N_-}{\Omega_1^U - \Omega_0^U - \sqrt{(\Omega_0^U - \Omega_1^U)^2 + 4N_-^2 \Omega_0^U \Omega_1^U}}, 1 \right]^T. \quad (75)$$

The real and imaginary parts of Ω_0 and Ω_1, giving the frequency shift and growth rate respectively, are shown in Figs. 3(a) and 3(b), for the case where the coupled-bunch instability is driven by the HOMs listed in Table II, where $\Omega_0^U = (78.4, 589.5) \text{ s}^{-1}$ and $\Omega_1^U = (-237.9, -21.8) \text{ s}^{-1}$. In Fig. 3(c), the comparison of the growth rates of mode 0 given by Eq. (73) as a function of N_0/N with SPACE simulations shows good agreement. The numerical growth rate is found by fitting the envelope of the betatron oscillations of the bunch centroids with an exponential function. For a discussion in the uniform filling pattern case see [11]. In the uniform filling pattern case, $N_0 = N_1 = N$, thus $N_- = 0$ and Eq. (48) reads

$$\begin{pmatrix} \tilde{x}_0^g(t) \\ \tilde{x}_1^g(t) \end{pmatrix} = c_0 \begin{pmatrix} 1 \\ 0 \end{pmatrix} e^{-i(\omega_\beta + \Omega_0^U)t} + c_1 \begin{pmatrix} 0 \\ 1 \end{pmatrix} e^{-i(\omega_\beta + \Omega_1^U)t}.$$

In the case $N_0 = 0$ and $N_0 = 2N$ we recover the single bunch case ($M = 1$) with $2N$ particles per bunch observing that one eigenvalue is zero and the other equal to $\Omega_0^U + \Omega_1^U = \Omega^U$, where Ω^U is the complex frequency shift of a single circulating bunch.

2. Elementary case 2: Three bunches

In the case $M = 3$ we discuss the configuration $N_0 = N_1 = 3N/2$, $N_2 = 0$, with $3N = N_T$, which describes a configuration with a missing bunch. The corresponding eigenvalue problem defined by Eq. (46) reads

$$|\mathbf{B} - \Omega\mathbf{I}| = \begin{vmatrix} \Omega_0^U - \Omega & a\Omega_0^U & a^*\Omega_0^U \\ a^*\Omega_1^U & \Omega_1^U - \Omega & a\Omega_1^U \\ a\Omega_2^U & a^*\Omega_2^U & \Omega_2^U - \Omega \end{vmatrix} = 0,$$

$$a = \frac{1 + \sqrt{3}i}{2},$$
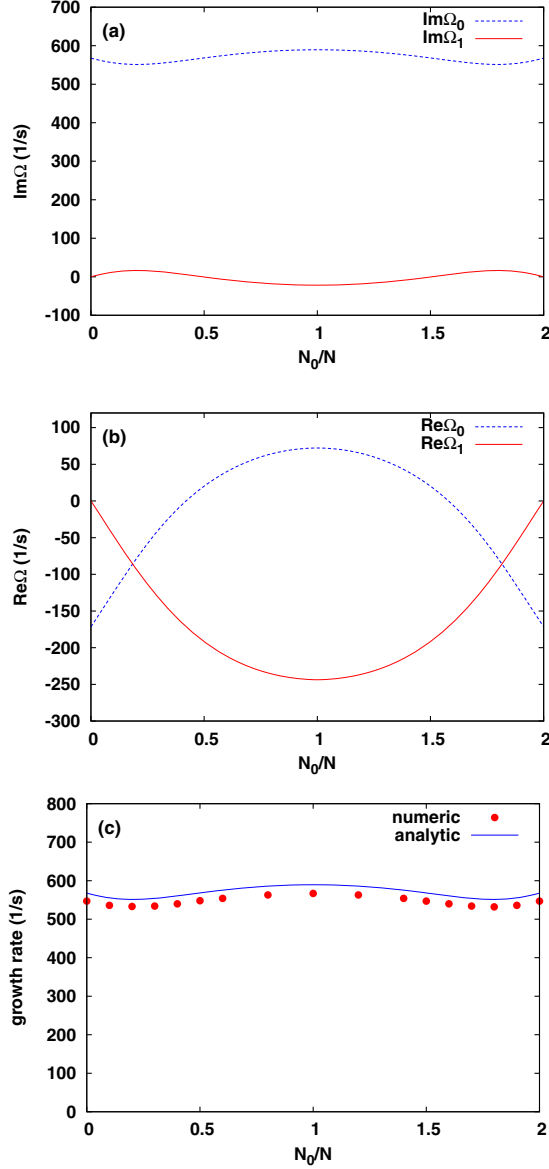
where $*$ denotes complex conjugate. It follows that

FIG. 3.   (a) Imaginary part (growth rate) and (b) Real part (frequency shift) of the modes Ω_0 and Ω_1, given by Eq. (73), for the case of two bunches ($M = 2$). N_0 and N_1 are the number of particles per bunch, and satisfy $N_0 + N_1 = 2N$, where N is the number of particles per bunch in the uniform filling pattern case ($N_0 = N_1 = N$). For $N_0 = 0$ and $N_0 = 2$ the system of two bunches degenerates in the system describing one bunch with $2N$ particles. The most unstable configuration is the configuration with the uniform filling pattern. (c) Comparison of the growth rates of mode 0 given by Eq. (73) as a function of N_0/N with SPACE self-consistent simulations, showing close agreement.

$$|\mathbf{B} - \Omega\mathbf{I}| = -\Omega\left[\Omega^2 - \mathbf{Tr}\,\mathbf{B}\Omega + \frac{3}{4}(\Omega_0^U\Omega_1^U + \Omega_0^U\Omega_2^U \right.$$

$$\left. + \Omega_1^U\Omega_2^U)\right] = 0, \qquad (76)$$

where $\mathbf{Tr}\,\mathbf{B} = \Omega_0^U + \Omega_1^U + \Omega_2^U$. Thus the eigenvalues read

$$\Omega_{0,1} = \frac{\mathbf{Tr}\,\mathbf{B}}{2}$$

$$\pm \frac{1}{2}\sqrt{(\mathbf{Tr}\,\mathbf{B})^2 - 3(\Omega_0^U\Omega_1^U + \Omega_0^U\Omega_2^U + \Omega_1^U\Omega_2^U)}.$$

$$\Omega_2 = 0. \qquad (77)$$

We notice that with the above configuration of one missing bunch, one of the eigenvalue is zero, thus there are two independent modes of oscillations. However, since the multibunch configuration is not symmetric, the eigenvalues differ from the eigenvalues of the uniform filling pattern case with $M = 2$. For comparison with the parameters used in the $M = 2$ case, the values of Ω_0 and Ω_1 in Eq. (77) are $\Omega_0 = (743.3, -517.8)\,\text{s}^{-1}$ and $\Omega_1 = (-905.7, 1085.5)\,\text{s}^{-1}$, to be compared with $\Omega_0^U = (78.4, 589.5)\,\text{s}^{-1}$ and $\Omega_1^U = (-237.9, -21.8)\,\text{s}^{-1}$ of the $M = 2$ case. The case $M = 3$ with $N_0 = 3N, N_1 = N_2 = 0$, degenerates, as for $M = 2$, in the case of one circulating bunch ($M = 1$), by observing that $\Omega_0 = \mathbf{Tr}\,\mathbf{B} = \Omega_0^U + \Omega_1^U + \Omega_2^U = \Omega^U$, and $\Omega_1 = \Omega_2 = 0$, where Ω^U is the complex frequency shift for $M = 1$. Extending this result to the case of arbitrary M, we conclude that

$$\sum_{\mu=0}^{M-1} \Omega_\mu = \mathbf{Tr}\,\mathbf{B} = \Omega^U. \qquad (78)$$

This result can be proved from Eq. (47) by observing that

$$\sum_{\mu=0}^{M-1} \Omega_\mu = \sum_{\mu=0}^{M-1} \Omega_\mu^U$$

$$= -i\frac{I_{av}c}{4\pi(E_0/e)\nu_\beta}\sum_{p=-\infty}^{+\infty}\sum_{\mu=0}^{M-1}|\tilde{\lambda}(pM\omega_0 + \mu\omega_0 + \omega_\beta)|^2$$

$$\times Z_1^\perp[pM\omega_0 + \mu\omega_0 + \omega_\beta]$$

$$= -i\frac{I_{av}c}{4\pi(E_0/e)\nu_\beta}\sum_{p=-\infty}^{+\infty}|\tilde{\lambda}(p\omega_0 + \omega_\beta)|^2 Z_1^\perp(p\omega_0 + \omega_\beta)$$

$$= \Omega^U, \qquad (79)$$

where we used $I_b = I_{av}/M$, since the average current I_{av} is assumed to be independent of M. We conclude by observing that Ω_1 is the eigenvalue with largest positive imaginary part, thus driven the fastest coupled-bunch instability of the configuration with $N_0 = N_1 = 3N/2$, $N_2 = 0$. Its imaginary part is $\text{Im}\Omega_1 = 1085.5\,\text{s}^{-1}$. On the other hand, the complex frequency shifts Ω_μ^U for the uniform filling pattern case with $M = 3$ are

$$\Omega_0^U = (-1168.7, 1041.6)\,\text{s}^{-1},$$

$$\Omega_1^U = (238.7, 401.3)\,\text{s}^{-1},$$

$$\Omega_2^U = (767.6, -875.2)\,\text{s}^{-1}.$$

We can therefore state that the fastest instability driven by the uniform filling pattern case, given by $\text{Im}\,\Omega_0 = 1041.6 \text{ s}^{-1}$, is slower than the fastest instability driven by the configuration with $N_0 = N_1 = 3N/2$, $N_2 = 0$.

3. Practical case 1: Uniform bunch train with a gap

We now consider the effect of a gap g in the uniform filling pattern with $M = h = 1320$, where h is the harmonic number. The number of bunches in the nonuniform filling pattern is $M_g = M - g$, and the number of particles per bunch is $N_g = N_T/M_g$, where $N_T = NM$ is the total number of particles in the train. The growth rate of bunch mode μ for the uniform filling case ($g = 0$) is plotted in Fig. 4. The blue circles show the analytical result, while the red squares show the numerical result obtained with SPACE for the modes $\mu = 1170$, 944 and 316 with the largest (absolute) growth rate value. In Fig. 5(a) we plot bunch trains for different gaps. Notice that the area of the rectangles is constant and equal to the total number of particles N_T. In Fig. 6 we plot the eigenvalue with the largest imaginary part, found by solving numerically the eigenvalue problem defined by Eq. (46), as a function of the number of bunches M_g. The comparison of the result with SPACE simulations shows a close agreement in this case as well. The eigenvalue with the largest imaginary part shown in Fig. 6 is very close to the growth rate of the fastest unstable mode $(1/\tau)_\mu^U = 1119 \text{ s}^{-1}$, $\mu = 1170$, over a large range of the gap g.

4. Practical case 2: Uniform bunch train with fluctuations in the bunch population

We now consider the effect of fluctuations in the bunch population N_m on a uniform bunch train with $M = h = 1320$. The bunch population N_m is generated assuming $N_m = N(1 + X_m)$, where X_m is a random
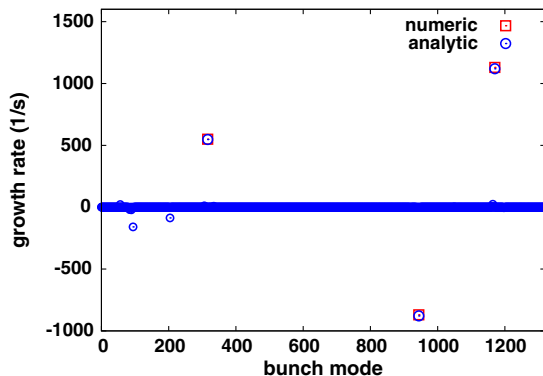

FIG. 4. Growth rates of bunch modes μ for the uniform filling pattern case with $M = h = 1320$, calculated analytically (blue circle) and numerically with SPACE (red square) showing close agreement. The numerical results are shown only for the three modes, $\mu = 1170$, 944 and 316, with the largest absolute value of the growth rate.
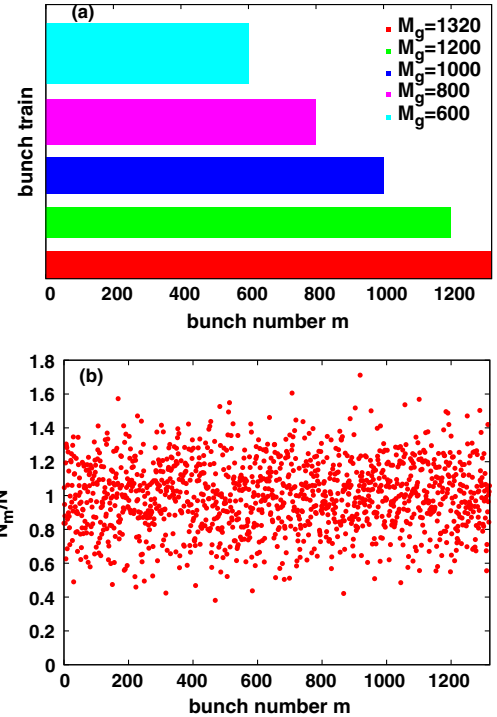

FIG. 5. (a) Bunch trains for different gaps g with number of bunches $M_g = M - g$, where $M = 1320$. The area of the rectangles equals the total number of particles in the uniform bunch train $N_T = NM$. (b) Single realization of a bunch train with bunch population $N_m = N(1 + X_m)$, where N_m is the bunch population of the uniform bunch train and X_m is a random variable with zero mean and variance $\sigma_X = 0.2$, corresponding to fluctuations in the bunch population of 20%.
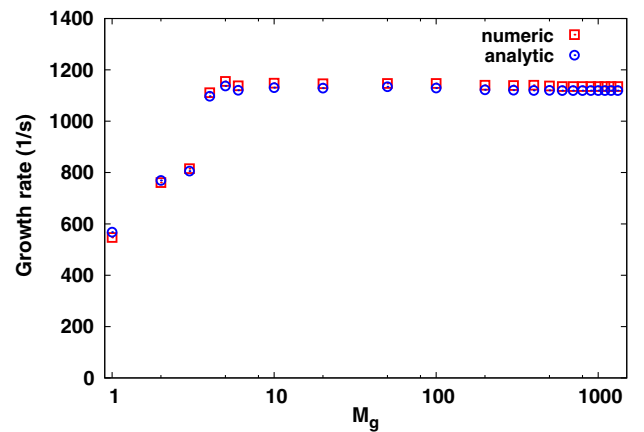

FIG. 6. Comparison of the eigenvalue with the largest imaginary part found by solving numerically the eigenvalue problem defined by Eq. (46) as a function of the number of bunches $M_g = M - g$, with SPACE numerical simulations, showing close agreement. Here g is the gap in the uniform filling pattern with $M = h = 1320$. The growth rate defined by the eigenvalue with the largest imaginary part is very close to the growth rate of the fastest unstable mode $(1/\tau)_\mu^U = 1119 \text{ s}^{-1}$, $\mu = 1170$ of the uniform filling pattern case over a large range of the gap g.

variable with zero mean and variance σ_X. Here we assume $\sigma_X = 0.2$, i.e., fluctuations in the bunch population of 20%. In Fig. 5(b) is shown one realization of the bunch configuration. The average value of the eigenvalue with the largest imaginary part, found by solving numerically the eigenvalue equation (46) is $\mathrm{Im}\Omega_\mu = (1122 \pm 0.1)$ s^{-1}, where $N_X = 10$ is the number of realizations of the random configurations. Notice the small value of the sample variance, $\sigma_s = 0.1$ s^{-1}, in the estimation of the average.

B. Fast eigenvalue estimation: The Gerschgorin circle theorem

For a rapid and efficient analysis of the eigenvalue problem, the application of the Gerschgorin circle theorem [37,38] offers a powerful method for the localization of the eigenvalues in the complex plane. The determination of the eigenvalue spectrum is very accurate in the limit of eigenvalue problems defined by strictly diagonally dominant matrices, where off-diagonal terms are small with respect to diagonal terms. More precisely, a $n \times n$ complex matrix $\mathbf{A} = (a_{ij})$ is diagonally dominant if each diagonal element in absolute value is greater than the sum of the absolute values of the off-diagonal elements in that row, i.e., the element of $\mathbf{A}$ satisfies

$$|a_{ii}| > \sum_{\substack{j=1 \\ j\neq i}}^{n} |a_{ij}|, \qquad 0 \leq i \leq n. \tag{80}$$

The application of Gerschgorin's theorem to a diagonally dominant matrix allows to state that each eigenvalue may not be too far from a diagonal element when the off-diagonal entries are small in norm [38]. In our case, since we look for perturbations around a uniform bunch train, we deal with matrices that are not far to be diagonally dominant. Gerschgorin's theorem precisely states that if λ is an eigenvalue of an $n \times n$ matrix $\mathbf{A} = (a_{ij})$, then, for some index i,

$$|\lambda - a_{ii}| \leq \sum_{\substack{j=1 \\ j\neq i}}^{n} |a_{ij}|, \qquad 0 \leq i \leq n. \tag{81}$$

The Gerschgorin row disks are accordingly defined as

$$\mathcal{G}_i(\mathbf{A}) = \left\{ z : z \in \mathbb{C} \quad \text{and} \quad |z - a_{ii}| \leq \sum_{\substack{j=1 \\ j\neq i}}^{n} |a_{ij}| \equiv r_i \right\}, \tag{82}$$

that is, for each row i, a Gerschgorin row disk is a closed disk in the complex plane with center at the diagonal element a_{ii}, and with radius r_i equal to the sum of the absolute values of the off-diagonal entries in the ith row. The notation $\mathcal{G}_i(\mathbf{A})[a_{ii}; r_i]$ can be used to denote the ith

Gerschgorin row disk with center a_{ii} and radius r_i. A number of corollaries follow from Gerschgorin's theorem, such as (1) every eigenvalue of $\mathbf{A}$ lies within at least one of the Gerschgorin row disks of $\mathbf{A}$, (2) the eigenvalues of $\mathbf{A}$ lie within the Gerschgorin column disks of $\mathbf{A}$ and, in the special case of diagonal matrices, (3) the Gerschgorin disks of $\mathbf{A}$ coincide with the eigenvalue spectrum if and only if $\mathbf{A}$ is a diagonal matrix. Corollary (2) follows from the fact that the eigenvalues of a matrix $\mathbf{A}$ are the same of its transpose $\mathbf{A}^T$, since they have the same characteristic equation $|\mathbf{A} - \lambda\mathbf{I}| = |\mathbf{A}^T - \lambda\mathbf{I}|$. The Gerschgorin column disks are defined similarly to the row case

$$\mathcal{G}_i(\mathbf{A}^T) = \left\{ z : z \in \mathbb{C} \quad \text{and} \quad |z - a_{ii}| \leq \sum_{\substack{j=1 \\ j\neq i}}^{n} |a_{ji}| \equiv c_i \right\}, \tag{83}$$

for each column i, for $1 \leq i \leq n$, with $\mathcal{G}_i(\mathbf{A}^T)[a_{ii}; c_i]$ denoting the ith Gerschgorin column disk with center a_{ii} and radius c_i. Since Gerschgorin's theorem states that all of the eigenvalues of the matrix $\mathbf{A}$ are contained both in the union of the row disks and in the union of the column disks, it follows that they must be in the intersection of the two regions,

$$\lambda \in \left(\bigcup_{i=1}^{n} \mathcal{G}_i(\mathbf{A}) \right) \cap \left(\bigcup_{i=1}^{n} \mathcal{G}_i(\mathbf{A}^T) \right). \tag{84}$$

As a consequence of corollary (3), if a Gerschgorin disk is disjoint from the other Gerschgorin disks, then it contains precisely one of the eigenvalues of $\mathbf{A}$, and, if the union of k Gerschgorin disks does not intersect any of the other $n - k$ disks, then there are exactly k eigenvalues (counting multiplicities) in the union of the k disks.

We are now in a position to apply the Gerschgorin circle theorem to the eigenvalue equation (46) defined by the matrix $\mathbf{B}$. In Fig. 7(a) we show the Gerschgorin column disks $\mathcal{G}_\mu(\mathbf{B}^T)$, for the case of a gap in the uniform filling pattern discussed in Fig. 6, where only the disks centered around Ω_μ^U with μ equal to 1170, 944 and 316 are shown, which correspond to the three eigenmodes of the uniform filling case with the largest growth rates, as shown in Fig. 4. Given the structure of the matrix $\mathbf{B}$, where each row μ is multiplied by Ω_μ^U, for the modes μ equal to 1170, 944 and 316, the radius of the Gerschgorin row disk is much larger than the radius of the Gerschgorin column disk, with the Gerschgorin column disks disjoint from each other for the cases with number of bunches $M_g = M - g$ equal to 1200, 1000, 800 and 600 shown by circles in blue, red, gray and green respectively in Fig. 7(a). Thus the circles represent the regions in the complex plane $\mathcal{G}_\mu(\mathbf{B}^T)[\Omega_\mu^U; c_\mu]$, centered at Ω_μ^U with radius c_μ, where the eigenvalues of the matrix $\mathbf{B}$ are located. By continuity [39] we can assert that the eigenvalues of $\mathbf{B}$ with the largest absolute value of the
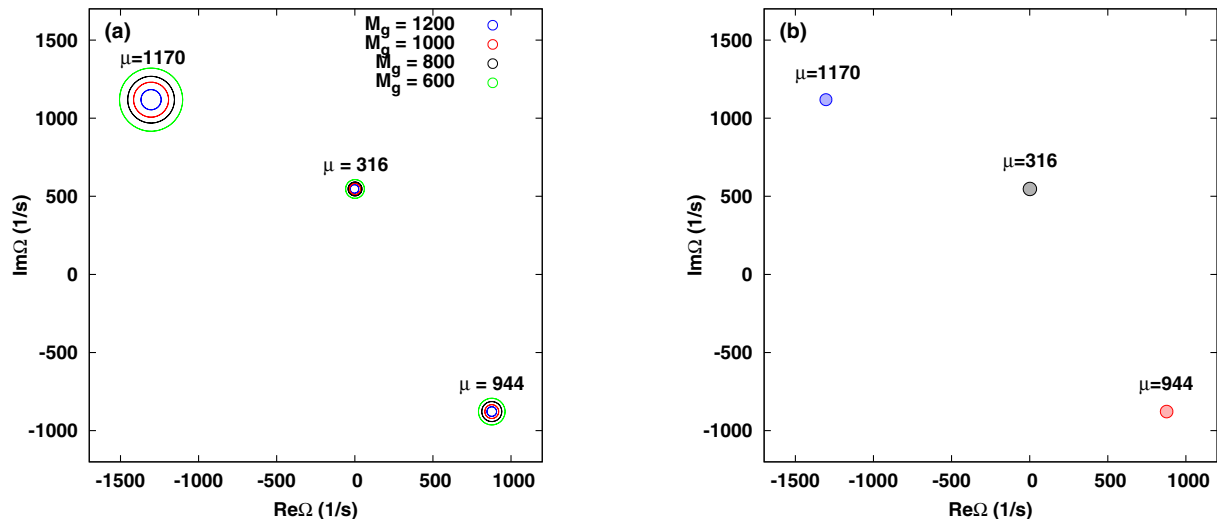
FIG. 7.   Gerschgorin circle theorem applied to: (a) a nonuniform filling pattern with $M_g = M - g$ bunches, where g is the gap in the uniform filling $M = 1320$, and (b) the case with fluctuations in the bunch population N_m on a uniform filling pattern with $M = 1320$. The regions determined by the intersection of the Gerschgorin disks, which, by the continuity of the eigenvalues [39], contain the three eigenvalues with the largest imaginary part, are shown with colored circles for the three fastest growing modes $\mu = 1170, 944, 316$ of the uniform filling case. In (a) the cases with $M_g = 1200$ (blue circle), $M_g = 1000$ (red circle), $M_g = 800$ (gray circle) and $M_g = 800$ (green circle) are shown. The radius of the Gerschgorin disks goes to zero in the limit of zero gap. In (b) the Gerschgorin disks for the same modes $\mu = 1170, 944, 316$ are shown with filled circles. Here the bunch population N_m is generated with a fluctuation of 20%.

imaginary part are located inside the circles centered at Ω_μ^U with μ equal to 1170, 944 and 316. The fastest instability is determined by the eigenvalue inside the circle centered at $\Omega_{1170}^U = (-1304, 1119)$ s^{-1}. The circle corresponding to $M_g = 600$ has the largest radius $c_{1170} = 202$ s^{-1}, with the imaginary part of the fastest unstable mode thus in the interval $[917, 1321]$ s^{-1}. This should be compared with the result 1122 s^{-1} from the numerical solution of the eigenvalue equation. Of course, the estimate is more precise for smaller values of the gap g. It is clear that the Gerschgorin circle theorem is particularly effective for the study of perturbations around the uniform filling pattern case. We remind here that computation of the radius of one Gerschgorin's disk is very fast, requiring M operations (sum over a row or a column of a $M \times M$ matrix).

The effectiveness of the Gerschgorin circle theorem is evident when applied to the practical case 2 studied in Sec. IV A, i.e., the case of a uniform bunch train with fluctuations in the bunch population N_m. Figure 7(b) shows the Gerschgorin column disks with center at Ω_μ^U, with μ equal to 1170, 944 and 316. The average radius and sample variance of each disk for $N_X = 100$ realizations of the random fluctuations is shown in Table III. The average

value of the radius of the disks is ≈ 40 s^{-1}, with a sample variance of ≈ 5 s^{-1}. We can therefore conclude that, in this case, the eigenvalues of **B** can be quickly estimated with very good accuracy, without the need to solve numerically the eigenvalue problem. This can be of great help for parametric scans or studies over a large number of realizations of the random fluctuations.

V. CONCLUSIONS

We discussed the SPACE, a parallel code for self-consistent beam dynamics simulations of collective effects driven by short- and long-range wakefields. For multibunch simulations, the long-range interaction is efficiently computed by a novel algorithm based on the expansion of the long-range wake function in Taylor series, allowing the calculation of the coupled-bunch interaction via storing few moments of the bunch densities. We presented an analytical treatment of the coupled-bunch instability for arbitrary filling patterns based on the formulation of an eigenvalue problem defined by the complex frequency shifts of the uniform filling pattern case. The numerical solution of the eigenvalue problem allows the study of instability thresholds via the determination of the eigenvalue with the largest imaginary part. The analysis is general and can be applied, for example, to study the stability of perturbations to a desired filling pattern due to fluctuations in the number of particles per bunch, or to find the most stable multibunch configuration by varying the number of particles per bunch under suitable constrains. As an application, we benchmarked theory and simulations for the case with a gap

TABLE III.   Gerschgorin column disks for practical case 2.

Mode (μ)	Center (Ω_μ^U), s^{-1}	Average radius, s^{-1}	Sample variance, s^{-1}
1170	$(-1304, 1119)$	38.1	4.1
944	$(877, -878)$	40.1	5.3
316	$(1.7, 547.2)$	43.3	5.5

in the uniform filling pattern, with parameters of the NSLS-II storage ring, and found that the coupled-bunch instability growth rate is weakly dependent on the gap, if the number of bunches is greater than 5 of the total 1320 rf buckets. For the case of a uniform filling pattern with fluctuations in the bunch population, we found that the numerical solution of the eigenvalue problem gives as well a result very close to the uniform filling pattern case, for a fluctuation in the bunch population of 20 percent. Lastly, we discussed the application of the Gerschgorin circle theorem, as a powerful tool for a rapid estimation of the eigenvalue spectrum, effective in particular for an accurate estimation of the eigenvalues in perturbative studies of uniform filling patterns.

ACKNOWLEDGMENTS

APPENDIX A: PROOF OF EQ. (37)

Multiplying Eq. (34) by $\exp(-i2\pi m\mu/M)$ and summing over m, Eq. (37) is obtained with the use of Eqs. (35) and (36), the relation

$$x_{[m+k]}(t) = \frac{1}{M}\sum_{\mu'=0}^{M-1}\tilde{x}_{\mu'}(t)e^{i2\pi(m+k)\mu'/M}, \qquad \text{(A1)}$$

and the identity

$$\begin{aligned} e^{i2\pi k\mu'/M}\sum_{m=0}^{M-1}N_{[m+k]}e^{i2\pi m(\mu'-\mu)/M} \\ = e^{i2\pi k\mu/M}\sum_{m=0}^{M-1}N_{[m+k]}e^{i2\pi[m+k](\mu'-\mu)/M} \\ = e^{i2\pi k\mu/M}\sum_{m=0}^{M-1}N_m e^{i2\pi m(\mu'-\mu)/M}. \end{aligned} \qquad \text{(A2)}$$

APPENDIX B: COMPLEX FREQUENCY SHIFTS FOR UNIFORM FILLING PATTERNS

Here we drop the superscript U in the complex frequency shifts Ω_μ^U, referring implicitly to the uniform filling pattern case.

1. Transverse case

In terms of the transverse impedance $Z_1^\perp$,

$$Z_1^\perp(\omega) = i\int_{-\infty}^{\infty}d\tau e^{i\omega\tau}W_1(\tau), \qquad \text{(B1)}$$

$$W_1(\tau) = -\frac{i}{2\pi}\int_{-\infty}^{\infty}d\omega e^{-i\omega\tau}Z_1^\perp(\omega), \qquad \text{(B2)}$$

the complex frequency shift Ω_μ given by Eq. (47) reads

$$\begin{aligned} \Omega_\mu = -i\frac{A_x N}{4\pi\omega_\beta}\int_{-\infty}^{\infty}d\omega|\tilde{\lambda}(\omega)|^2 Z_1^\perp(\omega) \\ \times \sum_{k=-\infty}^{+\infty}e^{ik[-\frac{\omega T_0}{M}+\frac{2\pi\mu}{M}+\frac{\omega_\beta T_0}{M}]}, \end{aligned} \qquad \text{(B3)}$$

where we used the fact that $W_1(\tau) = 0$ for $\tau < 0$ and $T_0 = C/c$. Using the identity

$$\sum_{k=-\infty}^{+\infty}e^{ikz} = 2\pi\sum_{p=-\infty}^{+\infty}\delta(z-2\pi p), \qquad \text{(B4)}$$

it follows

$$\begin{aligned} \Omega_\mu = -i\frac{A_x N}{2\omega_\beta}\sum_{p=-\infty}^{+\infty}\int_{-\infty}^{\infty}d\omega|\tilde{\lambda}(\omega)|^2 Z_1^\perp(\omega) \\ \times \delta\left[-\frac{\omega T_0}{M}+\frac{2\pi\mu}{M}+\frac{\omega_\beta T_0}{M}-2\pi p\right]. \end{aligned} \qquad \text{(B5)}$$

Changing integration variable $\bar{\omega} = \omega T_0/M$, $d\omega = M/T_0 d\bar{\omega}$, we have

$$\begin{aligned} \Omega_\mu = -i\frac{I_b Mc}{4\pi(E_0/e)\nu_\beta}\sum_{p=-\infty}^{+\infty}|\tilde{\lambda}(pM\omega_0+\mu\omega_0+\omega_\beta)|^2 \\ \times Z_1^\perp[pM\omega_0+\mu\omega_0+\omega_\beta], \end{aligned} \qquad \text{(B6)}$$

where we used $\omega_0 = 2\pi/T_0$, $A_x = ec/[\gamma T_0(E_0/e)]$, $I_b = eN/T_0$ and $\nu_\beta = \omega_\beta/\omega_0$. Thus the mode frequency shift ω_r and growth rate $1/\tau$ read

$$\begin{aligned} \omega_{r,\mu} = \frac{I_b Mc}{4\pi(E_0/e)\nu_\beta}\sum_{p=-\infty}^{+\infty}|\tilde{\lambda}(pM\omega_0+\mu\omega_0+\omega_\beta)|^2 \\ \times \text{Im}Z_1^\perp(pM\omega_0+\mu\omega_0+\omega_\beta), \end{aligned} \qquad \text{(B7)}$$

$$\begin{aligned} \tau_\mu^{-1} = -\frac{I_b Mc}{4\pi(E_0/e)\nu_\beta}\sum_{p=-\infty}^{+\infty}|\tilde{\lambda}(pM\omega_0+\mu\omega_0+\omega_\beta)|^2 \\ \times \text{Re}Z_1^\perp(pM\omega_0+\mu\omega_0+\omega_\beta). \end{aligned} \qquad \text{(B8)}$$

2. Longitudinal case

In terms of the longitudinal impedance $Z_0^\parallel$,

$$Z_0^\parallel(\omega) = \int_{-\infty}^{\infty}\frac{dz}{c}e^{i\omega z/c}W_0'(z), \qquad \text{(B9)}$$

$$W_0'(z) = \frac{1}{2\pi} \int_{-\infty}^{\infty} d\omega e^{-i\omega z/c} Z_0^{\parallel}(\omega), \tag{B10}$$

$$W_0''(z) = -\frac{i}{2\pi c} \int_{-\infty}^{\infty} d\omega \omega e^{-i\omega z/c} Z_0^{\parallel}(\omega), \tag{B11}$$

the complex frequency shift Ω_μ given by Eq. (67) reads

$$\Omega_\mu = i \frac{A_z N c}{4\pi\omega_s} \int_{-\infty}^{\infty} d\omega \omega |\tilde{\lambda}_0(\omega)|^2 Z_0^{\parallel}(\omega)$$
$$\times \sum_{k=-\infty}^{+\infty} e^{ik[-\frac{\omega T_0}{M} + \frac{2\pi\mu}{M} + \frac{\omega_s T_0}{M}]}, \tag{B12}$$

where we used the fact that $W_0'(z) = 0$ for $z < 0$ and $T_0 = C/c$. Using the identity given by Eq. (B4) it follows

$$\Omega_\mu = i \frac{A_z N c}{2\omega_s} \sum_{p=-\infty}^{+\infty} \int_{-\infty}^{\infty} d\omega \omega |\tilde{\lambda}(\omega)|^2 Z_0^{\parallel}(\omega) \delta$$
$$\times \left[-\frac{\omega T_0}{M} + \frac{2\pi\mu}{M} + \frac{\omega_s T_0}{M} - 2\pi p \right]. \tag{B13}$$

Changing integration variable $\bar{\omega} = \omega T_0/M$, $d\omega = M/T_0 d\bar{\omega}$, we have

$$\Omega_\mu = i \frac{I_b M \eta}{4\pi(E_0/e)\nu_s} \sum_{p=-\infty}^{+\infty} (pM\omega_0 + \mu\omega_0 + \omega_s)$$
$$\times |\tilde{\lambda}(pM\omega_0 + \mu\omega_0 + \omega_s)|^2 Z_0^{\parallel}(pM\omega_0 + \mu\omega_0 + \omega_s), \tag{B14}$$

where we used $\omega_0 = 2\pi/T_0$, $A_z = e\eta/(cT_0 E_0)$, $I_b = eN/T_0$ and $\nu_s = \omega_s/\omega_0$. Thus the mode frequency shift ω_r and growth rate $1/\tau$ read

$$\omega_{r,\mu} = -\frac{I_b M \eta}{4\pi(E_0/e)\nu_s} \sum_{p=-\infty}^{+\infty} (pM\omega_0 + \mu\omega_0 + \omega_s)$$
$$\times |\tilde{\lambda}(pM\omega_0 + \mu\omega_0 + \omega_s)|^2$$
$$\times \text{Im} Z_0^{\parallel}(pM\omega_0 + \mu\omega_0 + \omega_s), \tag{B15}$$

$$\tau_\mu^{-1} = \frac{I_b M \eta}{4\pi(E_0/e)\nu_s} \sum_{p=-\infty}^{+\infty} (pM\omega_0 + \mu\omega_0 + \omega_s) |\tilde{\lambda}(pM\omega_0$$
$$+ \mu\omega_0 + \omega_s)|^2 \text{Re} Z_0^{\parallel}(pM\omega_0 + \mu\omega_0 + \omega_s). \tag{B16}$$

[1] M. Migliorati and L. Palumbo, Multibunch and multi-particle simulation code with an alternative approach to wakefield effects, Phys. Rev. ST Accel. Beams **18,** 031001 (2015).

[2] M. Blaskiewicz, Report No. BNL-77074-2006-IR, 2006.

[3] J. M. Byrd, S. De Santis, G. Stover, D. Teytelman, J. Fox, J. Jacob, V. Serriere, and M. Georggson, Report No. SLAC-PUB-9367, 2002.

[4] R. Nagaoka, in *Proceedings of the 10th European Particle Accelerator Conference, Edinburgh, Scotland, 2006* (EPS-AG, Edinburgh, Scotland, 2006), THPCH032; R. Nagaoka, R. Bartolini, and J. Rowland, in *Proceedings of the 23rd Particle Accelerator Conference, Vancouver, Canada, 2009* (IEEE, Piscataway, NJ, 2009), FR5RFP046.

[5] G. Skripka, R. Nagaoka, M. Klein, F. Cullinan, and P. Tavares, Simultaneous computation of intrabunch and interbunch collective beam motions in storage rings, Nucl. Instrum. Methods Phys. Res., Sect. A **806,** 221 (2016).

[6] K. M. Hock and A. Wolski, Time evolution of coupled-bunch modes from beta function variation in storage rings, Phys. Rev. ST Accel. Beams **10,** 084401 (2007).

[7] A. Koschik, Ph.D. thesis, Technical University Graz, 2004.

[8] N. Mounet, Ph.D. thesis, EPFL, Lousanne, 2012.

[9] G. Bassi, A. Blednykh, and S. Krinsky, in *Proceedings of the 3rd International Particle Accelerator Conference, New Orleans, LA, 2012* (IEEE, Piscataway, NJ, 2012), TUPPP042.

[10] M. Klein and R. Nagaoka, in *Proceedings of the 4th International Particle Accelerator Conference, IPAC-2013, Shanghai, China, 2013* (JACoW, Shanghai, China, 2013), MOPWO003; R. Nagaoka (private communication).

[11] G. Bassi, A. Blednykh, W. Cheng, F. Gao, J. Rose, and D. Teytelman, Analysis of coupled-bunch instabilities for the NSLS-II storage ring with a 500 MHz 7-cell PETRA-III cavity, Nucl. Instrum. Methods Phys. Res., Sect. A **810,** 151 (2016).

[12] In our previous numerical work we called our code OASIS (optimal algorithm for self-consistent instabilities simulations) [11]. We are now aware that the same acronym is used for the open architecture software integration system (OASIS™) by G. H. Gillespie and B. W. Hill for the suite of software applications Particle Beam Optics Laboratory (PBO Lab™) [13]. We therefore changed the name of our code to SPACE (self-consistent parallel algorithm for collective effects). The reader should be aware that OASIS was the code name used in all our publications to date.

[13] G. H. Gillespie and B. W. Hill, in *Proceedings of the 22nd Particle Accelerator Conference, PAC-2007, Albuquerque, NM, 2007* (IEEE, Piscataway, NJ, 2007), THPAS037.

[14] G. Bassi and A. Blednykh, *Proceedings of the 24th Particle Accelerator Conference, PAC-2011, New York, 2011* (IEEE, New York, 2011), THP193.

[15] G. Bassi and A. Blednykh, Passive Landau cavity effects in arbitrary filling patterns (to be published); G. Bassi and A. Blednykh, in *Proceedings of the 25th Particle Accelerator Conference, PAC-2013, Pasadena, CA, 2013* (IEEE, New York, 2013), MOPBA03.

[16] G. Bassi, A. Blednykh, S. Krinsky, and J. Rose, in *Proceedings of the 3rd International Particle Accelerator Conference, New Orleans, LA, 2012* (IEEE, Piscataway, NJ, 2012), TUPPP043.

[17] In standard applications, where different bunches have a similar bunch population, the number of simulation

particles N_p is the same for all bunches. Of course, in extreme conditions such as studies of large variations in the bunch population, N_p should be chosen accordingly as a function of the number of particles N_m of bunch m, to allow for a proper numerical accuracy.

[18] R. L. Warnock and J. A. Ellison, Report No. SLAC-PUB-8404, 2000.

[19] M. Venturini, Microbunching instability in single-pass systems using a direct two-dimensional Vlasov solver, Phys. Rev. ST Accel. Beams **10,** 104401 (2007); M. Venturini, R. Warnock, and A. Zholents, Vlasov solver for longitudinal dynamics in beam delivery systems for x-ray free electron lasers, Phys. Rev. ST Accel. Beams **10,** 054403 (2007).

[20] G. Bassi, J. A. Ellison, K. Heinemann, and R. Warnock, Microbunching instability in a chicane: Two-dimensional mean field treatment, Phys. Rev. ST Accel. Beams **12,** 080704 (2009).

[21] B. Terzić and G. Bassi, New density estimation methods for charged particle beams with applications to microbunching instability, Phys. Rev. ST Accel. Beams **14,** 070701 (2011).

[22] G. Bassi, A. Blednykh, Y. Hidaka, and V. Smaluk, Decoherence effects and the slow head-tail damping (to be published).

[23] B. W. Zotter and S. A. Kheifets, *Impedances and Wakes in High-Energy Particle Accelerators* (World Scientific, Singapore, 1998).

[24] S. M. Ross, *Simulation* (Harcourt Academic Press, San Diego, 1997).

[25] S. G. Johnson and M. Frigo, A modified split-radix FFT with fewer arithmetic operations, IEEE Trans. Signal Process. **55,** 111 (2007).

[26] J. W. Cooley and J. W. Tuckey, An algorithm for the machine calculation of complex Fourier series, Math. Comput. **19,** 297 (1965).

[27] R. Yavne, in *Proceedings of the AFIPS Fall Joint Computer Conference* (Thompson, Washington D.C., 1968), Vol. 33, pp. 115–125.

[28] https://www.nersc.gov.

[29] P. Wilson, High energy electron linacs; application to storage ring RF systems and linear colliders, AIP Conf. Proc. **87,** 450 (1981).

[30] A. Chao, *Physics of Collective Beam Instabilities in High Energy Accelerators* (John Wiley & Sons, New York, 1993).

[31] J. L. Laclare, CERN Report No. 87-03, Vol. **I,** 1987.

[32] B. Zotter and F. Sacherer, CERN Report No. 77-13, 1977.

[33] R. D. Kohaupt, Report No. DESY-85-139, 1985.

[34] J. S. Berg, Ph.D. thesis, Stanford University, 1996.

[35] S. Prabhakar, New diagnostic and cures for coupled-bunch instabilities, Report No. SLAC-R-554, 2000; S. Prabhakar, J. D. Fox, and D. Teytelman, Curing Coupled-Bunch Instabilities with Uneven Fills, Phys. Rev. Lett. **86,** 2022 (2001).

[36] R. L. Graham, D. E. Knuth, and O. Patashnik, Integer functions, in *Concrete Mathematics: A Foundation for Computer Science*, 2nd ed. (Addison-Wesley, Reading, MA, 1994), Chap. 3, pp. 67–101.

[37] S. Gerschgorin, Über die Abgrenzung der Eigenwerte einer Matrix, *Bulletin de l'Académie des Sciences de l'URSS. Classe des sciences mathématiques et na* **7,** 749 (1931).

[38] W. Cheney and D. Kincaid, *Linear Algebra: Theory and Applications* (Jones & Bartlett Publishers, Sudbury, MA, 2010).

[39] The continuity of the eigenvalues follows from a classical result of complex analysis which states that the roots of a polynomial vary continuously with the coefficients. Since the coefficients of the characteristic polynomial $p(\lambda)$ of a matrix **A** can be expressed in terms of sum of principal minors, it follows that the coefficients of $p(\lambda)$ vary continuously with the entries of **A**. Consequently, the eigenvalues of **A** must vary continuously with the entries of **A** [C. D. Meyer, *Matrix Analysis and Applied Linear Algebra* (SIAM, Philadelphia, 2000), p. 497].